

Diffractive dijet photoproduction in ultraperipheral collisions at the LHC in next-to-leading order QCD

V. Guzey^a and M. Klasen^b

^a*National Research Center “Kurchatov Institute”, Petersburg Nuclear Physics Institute (PNPI), Gatchina, 188300, Russia*

^b*Institut für Theoretische Physik, Westfälische Wilhelms-Universität Münster, Wilhelm-Klemm-Straße 9, D-48149 Münster, Germany*

E-mail: vguzey@pnpi.spb.ru, michael.klasen@uni-muenster.de

ABSTRACT: We make predictions for the cross sections of diffractive dijet photoproduction in pp , pA and AA ultraperipheral collisions (UPCs) at the LHC during Runs 1 and 2 using next-to-leading perturbative QCD. We find that the resulting cross sections are sufficiently large and, compared to lepton–proton scattering at HERA, have an enhanced sensitivity to small observed momentum fractions in the diffractive exchange, commonly denoted z_P^{jets} , and an unprecedented reach in the invariant mass of the photon–nucleon system W . We examine two competing schemes of diffractive QCD factorization breaking, which assume either a global suppression factor or a suppression for resolved photons only and demonstrate that the two scenarios can be distinguished by the nuclear dependence of the distributions in the observed parton momentum fraction in the photon x_γ^{jets} .

Contents

1	Introduction	1
2	Diffractive dijet photoproduction in proton–proton UPCs at the LHC	2
2.1	General expression for the cross section	2
2.2	Flux of equivalent photons in pp UPCs	5
2.3	Results	8
3	Diffractive dijet photoproduction in proton–nucleus UPCs at the LHC	12
3.1	General expression for the cross section	12
3.2	Flux of equivalent photons in pA UPCs	13
3.3	Nuclear diffractive PDFs	14
3.4	Results	15
4	Diffractive dijet photoproduction in nucleus–nucleus UPCs at the LHC	19
4.1	General expression for the cross section	19
4.2	Flux of equivalent photons in AA UPCs	19
4.3	Results	20
5	Factorization breaking in diffractive dijet photoproduction	24
6	Conclusions	31
A	Suppression factors used for calculations in this paper	34

1 Introduction

Ultrapерipheral collisions (UPCs) of relativistic ions are characterized by large transverse distances (impact parameters) between the centers of the colliding ions, exceeding the sum of their radii. For such collisions, the strong interaction is suppressed and the ions interact electromagnetically through the emission of quasi-real photons [1–3]. The flux of these photons scales as Z^2 , where Z is the nuclear charge, and has a broad energy spectrum with the maximal photon energy in the laboratory frame scaling as γ_L , where γ_L is the nuclear Lorentz factor. This allows one to study photon–photon and photon–nucleus scattering at unprecedentedly high energies [4].

The UPC program at the LHC during Run 1 focused primarily on exclusive photoproduction of charmonia, in particular J/ψ and $\psi(2S)$ mesons, which probes the gluon distribution of the target $g(x, \mu^2)$ at small values of the momentum fraction x and a resolution scale $\mu^2 = \mathcal{O}(\text{few GeV}^2)$ [5]. This process was measured in proton–proton (pp) collisions at $\sqrt{s_{NN}} = 7$ TeV by the LHCb collaboration [6, 7], in proton–nucleus (pA)

collisions at $\sqrt{s_{NN}} = 5.02$ TeV by the ALICE collaboration [8], and in Pb-Pb collisions at $\sqrt{s_{NN}} = 2.76$ TeV by the ALICE collaboration [9–11] ($\sqrt{s_{NN}}$ is the invariant collision energy per nucleon). The analyses of these data at leading-order (LO) and next-to-leading order (NLO) QCD have provided new constraints on the small- x behavior of the gluon distribution in the proton $g_p(x, \mu^2)$ down to $x = 6 \times 10^{-6}$ [12, 13] and of the gluon distribution in heavy nuclei $g_A(x, \mu^2)$ down to $x \approx 10^{-3}$ [14, 15]. The data also restrict the parameters and the strong interaction dynamics of the color dipole model approach [16, 17] and the STARlight Monte Carlo generator [18].

The LHCb collaboration also measured exclusive photoproduction of Υ mesons in pp UPCs at $\sqrt{s_{NN}} = 7$ and 8 TeV [19]; in perturbative QCD (pQCD), these data probe the proton gluon distribution at the resolution scale $\mu^2 = \mathcal{O}(\text{few tens GeV}^2)$ [12]. In addition, coherent photoproduction of ρ mesons in nucleus–nucleus (AA) UPCs was measured by the STAR collaboration at RHIC at $\sqrt{s_{NN}} = 64.4, 130$ and 200 GeV [20–22] and by the ALICE collaboration at $\sqrt{s_{NN}} = 2.76$ TeV at the LHC [23]. These data probe the dynamics of soft high-energy γp and γA interactions, see e.g. Ref. [24].

Another potentially interesting process, which can be studied in pp , pA and AA UPCs at the LHC, is diffractive photoproduction of dijets, see Fig. 1. The measurement and the QCD analysis of this process in pp and pA UPCs will continue and extend the studies in lepton–proton scattering at HERA [25–33], giving a new handle on the key issue of factorization breaking and providing additional information on the proton diffractive PDFs. In AA (and to some degree pA) UPCs at the LHC, diffractive dijet photoproduction on nuclei presents an open field of research, which gives access to the novel unmeasured nuclear diffractive PDFs and the nuclear dependence of factorization breaking. Note that studies of diffractive dijet photoproduction in UPCs at the LHC are complimentary to those of diffractive dijet production in proton–antiproton scattering at the Tevatron [34, 35] and in proton–proton scattering at the LHC [36].

The outline of this paper is as follows: Sections 2, 3 and 4 contain our results for the pp , pA and AA cases, respectively, which we present in the same order. First, we give the general expression for the cross section of diffractive dijet photoproduction in the considered UPC. Then we discuss its main ingredients, i.e. the photon flux, the rapidity gap survival probability and the diffractive parton distributions. Third, we give and discuss our predictions for the cross sections of diffractive dijet photoproduction in UPCs in the LHC kinematics for Runs 1 and 2. In Sec. 5, we discuss diffractive QCD factorization breaking and study its effect on our predictions. Finally, we summarize our results in Sec. 6. For convenience, simple analytic fits to the suppression factors used in our calculations in the pp and pA cases are collected in the Appendix.

2 Diffractive dijet photoproduction in proton–proton UPCs at the LHC

2.1 General expression for the cross section

The mechanism of diffractive dijet photoproduction in ultraperipheral collisions of relativistic ions A and B is illustrated in Fig. 1. The figure shows the dominant leading-order (LO)

Feynman graphs for the direct (graph *a*) and the resolved (graph *b*) photon contributions to the production of two quark jets.

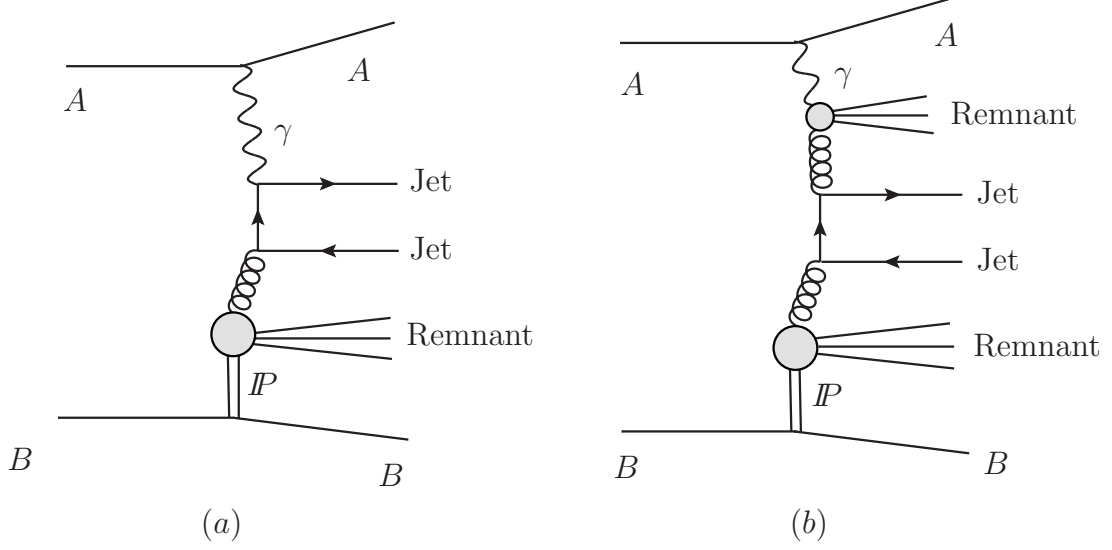


Figure 1. Typical leading-order Feynman graphs for diffractive dijet photoproduction in UPCs of hadrons A and B . Graphs *a* and *b* correspond to the direct and resolved photon contributions, respectively.

Considering proton–proton UPCs, $A = B = p$, the cross section of diffractive dijet photoproduction can be written as a sum of two terms:

$$d\sigma(pp \rightarrow p + 2\text{jets} + X' + Y) = d\sigma(pp \rightarrow p + 2\text{jets} + X' + Y)^{(+)} + d\sigma(pp \rightarrow p + 2\text{jets} + X' + Y)^{(-)}, \quad (2.1)$$

where X' stands for the produced diffractive final state X after removing two jets and Y denotes the final state of the diffracting proton, which, besides the elastic state $Y = p$, may contain hadronic states with low invariant mass. Note that the possibility of the proton diffraction dissociation is not explicitly shown in Fig. 1. The first and the second terms in Eq. (2.1) correspond to the diffracting proton moving along the positive and the negative z -axis, respectively. This reflects the ambiguity common for symmetric UPCs that either of the colliding ions can serve as a photon source and as a target [4]. Since the jet pseudorapidities η_1 and η_2 are usually defined with respect to the direction of the diffracting proton [37], the two terms in Eq. (2.1) can be related to each other by inverting the sign of η_1 and η_2 :

$$d\sigma(pp \rightarrow p + 2\text{jets} + X' + Y)^{(-)} = d\sigma(pp \rightarrow p + 2\text{jets} + X' + Y)^{(+)}_{|\eta_1 \rightarrow -\eta_1, \eta_2 \rightarrow -\eta_2}. \quad (2.2)$$

The cross section $d\sigma(pp \rightarrow p + 2\text{jets} + X' + Y)^{(+)}$ can be readily written by analogy with the standard expression for the dijet diffractive photoproduction cross section $d\sigma(ep \rightarrow$

$e + 2\text{jets} + X' + Y$) for lepton–proton scattering, see e.g. [37, 38]:

$$d\sigma(pp \rightarrow p + 2\text{jets} + X' + Y)^{(+)} = \sum_{a,b} \int_{t_{\text{cut}}}^{t_{\text{min}}} dt \int_{x_P^{\text{min}}}^{x_P^{\text{max}}} dx_P \int_0^1 dz_P \int_{y_{\text{min}}}^{y_{\text{max}}} dy \int_0^1 dx_\gamma \\ \times S^2(y) f_{\gamma/p}(y) f_{a/\gamma}(x_\gamma, \mu^2) f_{b/p}^{D(4)}(x_P, z_P, t, \mu^2) d\hat{\sigma}_{ab \rightarrow \text{jets}}^{(n)}, \quad (2.3)$$

where a and b are parton flavors; $f_{\gamma/p}(y)$ is the flux of equivalent photons of the proton, which depends on the photon light-cone momentum fraction y ; $f_{a/\gamma}(x_\gamma, \mu^2)$ is the parton distribution function (PDF) of the photon, which depends on the parton light-cone momentum fraction x_γ and the factorization scale μ ; $f_{b/p}^{D(4)}(x_P, z_P, t, \mu^2)$ is the diffractive PDF of the proton; $d\hat{\sigma}_{ab \rightarrow \text{jets}}^{(n)}$ is the elementary cross section for the production of an n -parton final state in the interaction of partons a and b ; and the sum over a involves quarks and gluons (the resolved photon contribution) and the direct photon contribution with $a = \gamma$, which has support at LO only at $x_\gamma = 1$.

In Eq. (2.3), besides the standard expression for ep scattering, we also explicitly introduced the rapidity gap survival factor of $S^2(y) \leq 1$, which takes into account the probability of soft inelastic interactions between the colliding protons, which populate, and thus suppress, the final-state rapidity gaps. The factor of $S^2(y)$ depends on y and the total invariant energy $\sqrt{s_{NN}}$; in pp UPCs, it can be viewed as a phenomenological factor modifying the photon flux $f_{\gamma/p}(y)$ [12, 39].

The QCD collinear factorization theorem for hard inclusive diffraction [40] allows one to introduce universal diffractive PDFs $f_{b/p}^{D(4)}(x_P, z_P, t, \mu^2)$ and to determine them by fitting to the measured diffractive structure functions [41–43]. The analysis also shows that for small values of x_P , $f_{b/p}^{D(4)}(x_P, z_P, t, \mu^2)$ can be written as the product of two factors [44]:

$$f_{b/p}^{D(4)}(x_P, z_P, t, \mu^2) = f_{b/P}(z_P, \mu^2) f_{P/p}(x_P, t), \quad (2.4)$$

where $f_{b/P}(z_P, \mu^2)$ is the PDF of the Pomeron (the lower blob in Fig. 1) and $f_{P/p}(x_P, t)$ is the Pomeron flux (the double line in Fig. 1). Note that the word “Pomeron” here denotes the diffractive exchange. Equation (2.4) helps to understand the meaning of the diffractive variables z_P , x_P and t entering Eq. (2.3): z_P is the light-cone momentum fraction of a parton in the Pomeron; x_P is the light-cone momentum fraction of the Pomeron in the proton; t is the invariant momentum transfer squared.

In the measurements of diffractive dijet photoproduction in ep scattering, the variables y , x_P and t are directly reconstructed by detecting the scattered electron, the final proton and the diffractive final state, see e.g. [27]:

$$y \equiv \frac{q \cdot p}{k \cdot p} = 1 - \frac{E'_e}{E_e}, \\ x_P \equiv \frac{q \cdot (p - p_Y)}{q \cdot p} = \frac{E_X + P_{X,z}}{2E_p} = \frac{M_X^2}{sy}, \\ t \equiv (p - p_Y)^2, \quad (2.5)$$

where p , p_Y , k , and q are the four-momenta of the initial proton, the final proton (with the possibility of diffraction dissociation into the state Y), the initial lepton and the photon,

respectively; E_e , E'_e , and E_X are the energies of the initial lepton, the final lepton, and the diffractive final state X , respectively; $P_{X,z}$ and M_X are the z -component of the momentum and the invariant mass of the state X , respectively; and $s = (k + p)^2$ is the square of the total center-of-mass energy of the collision. In ep scattering at HERA, the limits on y , x_P and t are determined by the experimental conditions and cuts. In contrast, in pp UPCs the scattered protons travel along the beam pipe, and, hence, are undetected. As a result, the limits on y , t and x_P in Eq. (2.3) are determined from general requirements to produce a diffractive final state.

The two remaining variables z_P and x_γ in Eq. (2.3) cannot be directly reconstructed by measuring the final state; their values can be compared to the hadron-level estimators z_P^{jets} and x_γ^{jets} , respectively, which are reconstructed from the measurement of the dijet and the diffractive final state [27]:

$$\begin{aligned} z_P^{\text{jets}} &= \frac{\sum_{\text{jets}} (E_i + P_{i,z})}{E_X + P_{X,z}}, \\ x_\gamma^{\text{jets}} &= \frac{\sum_{\text{jets}} (E_i - P_{i,z})}{E_X - P_{X,z}}, \end{aligned} \quad (2.6)$$

where the sum \sum_{jets} runs over the hadronic final states labeled “ i ”, which are included in the jets.

2.2 Flux of equivalent photons in pp UPCs

The flux of quasi-real photons emitted by a relativistic proton (ion) can be found using the well-known Weizsäcker–Williams (WW) approximation [1–3, 45, 46]. Since one also needs to take into account the charge and magnetization distribution in the proton, in practical applications one often uses approximate expressions [47, 48] reproducing the exact result with a few percent accuracy, see the discussion in Ref. [49].

The photon flux produced by a relativistic charge Z at the transverse distance b from its center reads, see e.g. [46]:

$$f_{\gamma/Z}(x, b) = \frac{\alpha_{\text{e.m.}} Z^2}{\pi^2} \frac{1 + (1 - x)^2}{2x} \left| \int_0^\infty \frac{dk_\perp k_\perp^2}{k_\perp^2 + (xm_p)^2} F_{ch}(k_\perp^2 + (xm_p)^2) J_1(bk_\perp) \right|^2, \quad (2.7)$$

where x is the fraction of the ion energy carried by the photon; $\alpha_{\text{e.m.}}$ is the fine-structure constant; $F_{ch}(k_\perp^2)$ is the charge form factor; k_\perp is the photon transverse momentum; J_1 is the Bessel function of the first kind; and m_p is the proton mass. Different expressions for the photon flux used in the literature correspond to various assumptions for $F_{ch}(k_\perp^2)$ and treatments of subleading terms in Eq. (2.7).

The integration of $f_{\gamma/Z}(x, b)$ over all impact parameters gives the following general expression for the photon flux produced by a relativistic ion:

$$f_{\gamma/Z}(x) = \frac{\alpha_{\text{e.m.}} Z^2}{\pi} \frac{1 + (1 - x)^2}{2x} \int_0^\infty dk_\perp^2 k_\perp^2 \left(\frac{F_{ch}(k_\perp^2 + (xm_p)^2)}{k_\perp^2 + (xm_p)^2} \right)^2. \quad (2.8)$$

In our calculations of pp UPCs we will use the result of Drees and Zeppenfeld (DZ) [47]:

$$f_{\gamma/p}(x) = \frac{\alpha_{\text{e.m.}}}{2\pi} \frac{1 + (1 - x)^2}{x} \left[\ln A - \frac{11}{6} + \frac{3}{A} - \frac{3}{2A^2} + \frac{1}{3A^3} \right], \quad (2.9)$$

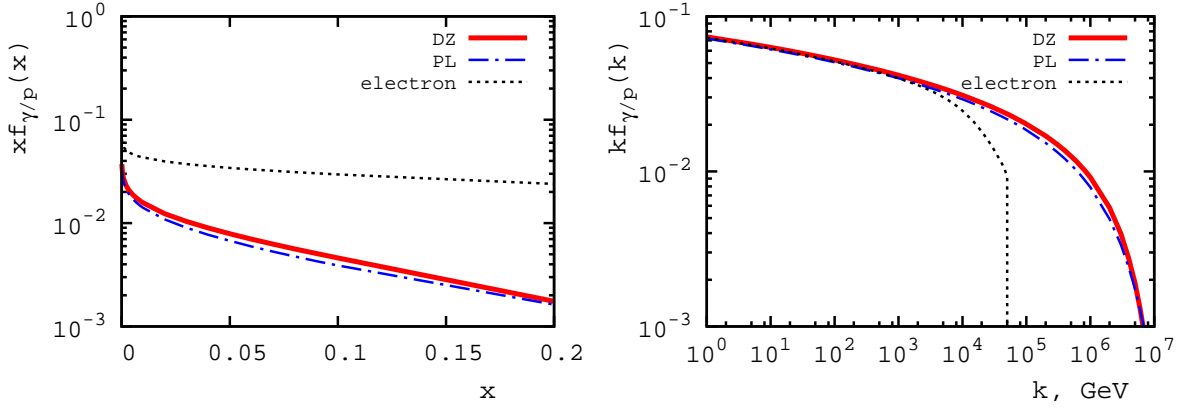


Figure 2. Left: The proton and electron photon spectra $xf_{\gamma/p}(x)$ and $xf_{\gamma/e}(x)$, respectively, as a function of the energy fraction x . Right: The photon spectra $kf_{\gamma/p}(k)$ and $kf_{\gamma/e}(k)$ as a function of the photon energy k in the target rest frame.

where $A = 1 + (0.71 \text{ GeV}^2)/Q_{\min}^2$ and $Q_{\min}^2 = (xm_p)^2/(1-x)$ is the minimal kinematically-allowed photon virtuality. Alternatively, in the literature one also considers the photon flux produced by a relativistic point-like (PL) charge Z passing a target at a minimum impact parameter b_{\min} :

$$f_{\gamma/Z}(x) = \frac{\alpha_{\text{e.m.}} Z^2}{\pi} \frac{1}{x} \left[2\zeta K_0(\zeta) K_1(\zeta) - \zeta^2 (K_1^2(\zeta) - K_0^2(\zeta)) \right], \quad (2.10)$$

where $\zeta = xm_p b_{\min}$ and $b_{\min} = 0.7 \text{ fm}$ for the proton [49].

It is illustrative to compare the photon flux of the proton with that of a relativistic electron [3]:

$$f_{\gamma/e}(x) = \frac{\alpha_{\text{e.m.}}}{2\pi} \left[\frac{1 + (1-x)^2}{x} \ln \frac{Q_{\max}^2(1-x)}{(m_e x)^2} + 2m_e^2 x \left(\frac{1}{Q_{\max}^2} - \frac{1-x}{(m_e x)^2} \right) \right], \quad (2.11)$$

where m_e is the electron mass; Q_{\max}^2 is the maximal photon virtuality, which is usually determined by the experimental conditions. Figure 2 presents a comparison of the spectrum of equivalent photons of the proton with that of the electron. In the left panel, we show $xf_{\gamma/p}(x)$ for the proton as a function of x (the red solid and the blue dot-dashed curves corresponding to Eqs. (2.9) and (2.10), respectively) and $xf_{\gamma/e}(x)$ for the electron (the dotted black curve corresponding to Eq. (2.11)). One can see from this panel that the energy spectrum for the point-like electron is much flatter than that for the composite proton. The photon energy k scales as $\gamma_L m_p$ in the laboratory frame and as $2\gamma_L^2 m_p$ in the target rest frame, where γ_L is the Lorentz factor of the emitting ion. The right panel of Fig. 2 shows the photon spectra $kf_{\gamma/p}(k)$ and $kf_{\gamma/e}(k)$ as a function of the photon energy k in the proton target rest frame. For the proton beam, the curves correspond to proton–proton collisions at $\sqrt{s_{NN}} = 7 \text{ TeV}$. For the electron beam, the curve corresponds to the HERA kinematics with the 27.5 GeV electron beam and the 920 GeV proton beam. One

can see from the panel that pp UPCs, in principle, allow one to obtain photon energies exceeding those at HERA by two orders of magnitude.

We explained in Sec. 2.1 that the photon flux $f_{\gamma/p}(x)$ is somewhat reduced by the rapidity gap survival probability factor of $S^2(x)$. To estimate it, we use the method of Refs. [12, 50], where $S^2(x)$ is calculated as a result of eikonalization of multiple Pomeron exchanges between the colliding protons:

$$S^2(x) = \frac{\int d^2b |\mathcal{M}(x, b)|^2 P(s, b)}{\int d^2b |\mathcal{M}(x, b)|^2}, \quad (2.12)$$

where b is the impact parameter; $\mathcal{M}(x, b)$ is the diffractive amplitude of the process of interest in the impact parameter space; $P(s, b)$ is the probability to not have the strong inelastic proton–proton interaction at the impact parameter b ; and $s = s_{NN}$ for brevity.

The probability $P(s, b)$ in the two-channel eikonal model of Ref. [50] is

$$P(s, b) = \frac{1}{4(1 - \gamma^2)} \left[(1 + \gamma)^3 e^{-(1+\gamma)^2 \Omega(s, b)} + (1 - \gamma)^3 e^{-(1-\gamma)^2 \Omega(s, b)} + 2(1 - \gamma^2) e^{-(1-\gamma^2) \Omega(s, b)} \right], \quad (2.13)$$

where $\gamma = 0.4$ and $\Omega(s, b)$ is the proton optical density. Assuming that $\Omega(s, b)$ has the form of the effective Pomeron exchange trajectory, one obtains:

$$\Omega(s, b) = \alpha \frac{\sigma_{pp}^{\text{tot}}(s)}{4\pi B_P} e^{-b^2/(4B_P)}, \quad (2.14)$$

where $\sigma_{pp}^{\text{tot}}(s)$ is the total proton–proton cross section; $B_P = B_0/2 + \alpha' \ln(s/s_0)$ is the slope of the t dependence of the elastic pp amplitude; and the parameter $\alpha \geq 1$ results from eikonalized multiple Pomeron exchanges and is found from the requirement:

$$\sigma_{pp}^{\text{tot}}(s) = 2 \int d^2b \left[1 - \frac{1}{4} e^{-(1+\gamma)^2 \Omega(s, b)/2} - \frac{1}{4} e^{-(1-\gamma)^2 \Omega(s, b)/2} - \frac{1}{2} e^{-(1-\gamma^2) \Omega(s, b)/2} \right]. \quad (2.15)$$

For $\sigma_{pp}^{\text{tot}}(s)$, we use the fit of the Review of Particle Physics [51]. The resulting values of $S^2(x)$ weakly depend on the exact value of the slope B_P ; in our calculation, we used $B_0 = 10 \text{ GeV}^{-2}$ and $\alpha' = 0.25 \text{ GeV}^{-2}$, which correctly reproduce the slope of the elastic pp cross section at small $|t|$ [50].

For $|\mathcal{M}(x, b)|^2$ in Eq. (2.12), we use the photon flux of the proton in the impact parameter space, Eq. (2.7), with $F_{ch}(Q^2) = F_p(Q^2) = 1/(1 + Q^2/(0.71 \text{ GeV}^2))^2$. Since the contribution of small impact parameters $b < b_{\min} \approx 0.7 \text{ fm}$ to the photon flux, Eq. (2.7), is small, the integrand in Eq. (2.12) receives the dominant contribution from $b > b_{\min}$, where $\Omega(s, b)$ is not large. As a result, one expects that the suppression due to $S^2(x)$ should not be large.

The resulting values of $S^2(x)$ as a function of the photon light-cone momentum fraction x are shown in Fig. 3. The red solid curve corresponds to $\sqrt{s_{NN}} = 7 \text{ TeV}$, and the blue dashed curve is for $\sqrt{s_{NN}} = 13 \text{ TeV}$. Since larger values of x correspond effectively to smaller values of the impact parameter b , where the suppression due to the strong interaction is stronger, $S^2(x)$ decreases with an increase of x . Also, the suppression somewhat

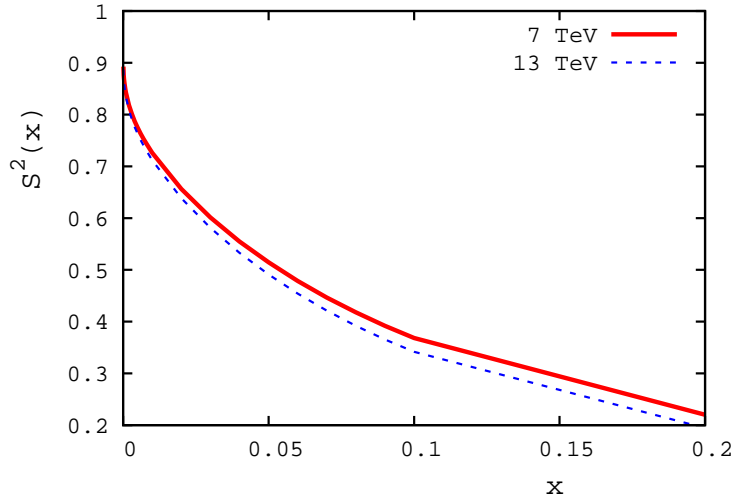


Figure 3. The rapidity gap survival probability $S^2(x)$ (2.12) as a function of the photon momentum fraction x for $\sqrt{s_{NN}} = 7$ TeV (red solid curve) and $\sqrt{s_{NN}} = 13$ TeV (blue dashed curve).

increases with an increase of the invariant collision energy $\sqrt{s_{NN}}$ as a result of the increase of $\sigma_{pp}^{\text{tot}}(s)$ and the optical density $\Omega(s, b)$. For convenience, a simple fit to the curves in Fig. 3 is given in the Appendix. Note that our values of $S^2(x)$ are consistent with the results for $S^2(x)$ for exclusive photoproduction of J/ψ and Υ mesons in pp UPCs [12] and also with the results of the calculation using a simpler model for the rapidity gap survival of Ref. [52].

2.3 Results

We performed next-to-leading order (NLO) pQCD calculations implementing the inclusive k_T -cluster algorithm [33] of the cross section of diffractive photoproduction of dijets in pp UPCs, Eq. (2.1), using the following cuts (compare to the cuts used, e.g., in Ref. [27]):

$$\begin{aligned}
&0 < y < 1, \\
&E_T^{\text{jet1}} > 20 \text{ GeV}, \quad E_T^{\text{jet2}} > 18 \text{ GeV}, \\
&-6 < \eta^{\text{jet1,2}} < 6, \\
&x_P \leq 0.03, \quad z_P^{\text{jets}} \leq 1, \\
&M_Y \leq 1.6 \text{ GeV}, \quad |t| < 1 \text{ GeV}^2,
\end{aligned} \tag{2.16}$$

where $E_T^{\text{jet1,2}}$ and $\eta^{\text{jet1,2}}$ are the transverse energies and the pseudorapidities of the two jets, respectively. For input, we used the DZ photon flux of the proton, Eq. (2.9), modified by the rapidity gap survival probability $S^2(y)$, Eq. (2.12), the GRV-HO photon PDFs [53], and the 2006 H1 proton diffractive PDFs (fit B) [42].

Figures 4 and 5 show the resulting diffractive dijet photoproduction cross sections for pp UPCs at $\sqrt{s_{NN}} = 7$ TeV and $\sqrt{s_{NN}} = 13$ TeV, respectively. Different panels present the cross section as a function of x_γ^{jets} , z_P^{jets} , E_T^{jet1} , the invariant mass of the photon-proton

system W , $\langle \eta^{\text{jets}} \rangle = (\eta_1 + \eta_2)/2$, $|\Delta \eta^{\text{jets}}| = |\eta_1 - \eta_2|$, the invariant mass of the dijet system M_{12} , and M_X , see [27]. The central thick solid lines show the result of the calculation, when the renormalization and factorization scale μ is identified with the transverse energy of jet 1, $\mu = E_T^{\text{jet1}}$; the dotted lines correspond to the calculation with $\mu = 2E_T^{\text{jet1}}$ and $\mu = (1/2)E_T^{\text{jet1}}$. Thus, the spread between the dashed lines quantifies the theoretical uncertainty of our NLO calculations associated with the choice of the factorization and renormalization scales. One can see from the figures that for our choice of $E_T^{\text{jet1}} > 20$ GeV, this uncertainty is rather insignificant.

Several features of the presented results merit discussion and comparison to diffractive dijet photoproduction in ep scattering at HERA [25–27]. First, the predicted yields are comparable to those observed in the ep case; the integrated cross section is $\mathcal{O}(\text{hundreds pb})$ at $\sqrt{s_{NN}} = 7$ TeV and $\mathcal{O}(\text{few nb})$ at $\sqrt{s_{NN}} = 13$ TeV. Second, while the general trends of the dependence on various variables are similar in the pp UPC and ep cases, the former allows to probe values of W exceeding those achieved in the ep case by at least a factor of ten and to produce dijets with the significantly larger M_{12} and M_X . In addition, the contribution of the low- z_P^{jets} region is much more important in the pp UPC case than in the ep case, which signals the enhanced sensitivity to the proton diffractive PDFs $f_{b/p}^{D(4)}(x_P, z_P, t, \mu^2)$ at small z_P , where they are poorly constrained [41–43].

It is interesting to speculate that the large cross section of diffractive dijet photoproduction in pp UPCs at small z_P^{jets} might contribute to hard diffractive dijet production in pp scattering at large $\log_{10}(x_P^-)$ and cause the dependence of the suppression factor parametrizing the rapidity gap survival probability on the momentum fraction of the parton in the Pomeron [35, 54].

In the experiment, to trigger on the events corresponding to diffractive dijet photoproduction in UPCs, one should employ the selection criteria typical for diffractive scattering in photoproduction: the absence of hadronic activity adjacent to the beam directions (presence of large rapidity gaps) will correspond to (very) small transverse momenta of the final-state protons (ions) and guarantee that the exchanged photon is quasi-real and that the photon–target interaction is diffractive; the detector will register two hard jets with large p_T and possibly the forward energy flow from the remnant diffractive final state (see Fig. 1).

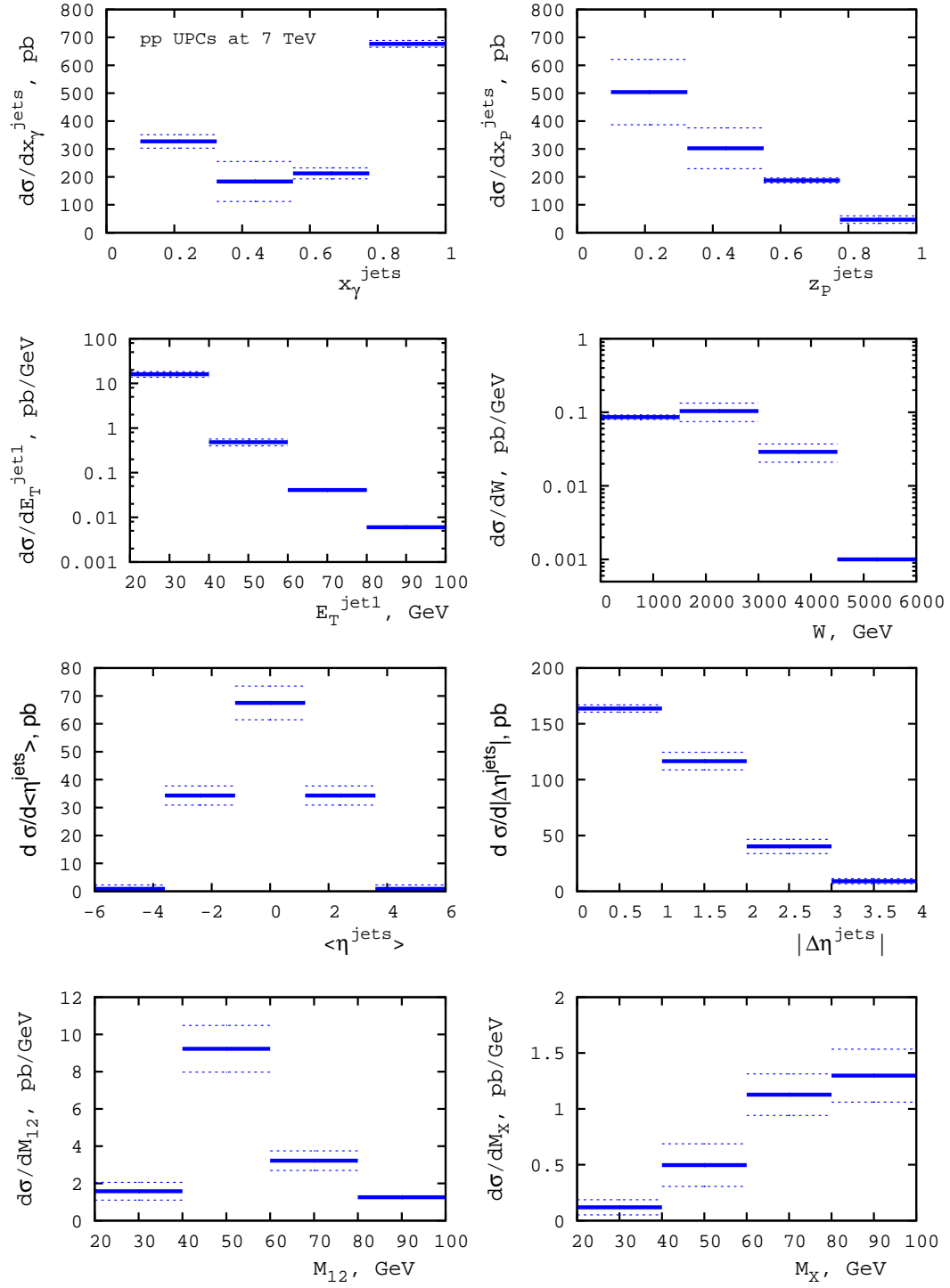


Figure 4. The differential cross section of diffractive photoproduction of dijets $d\sigma(pp \rightarrow p + 2\text{jets} + X' + Y)$ as a function of various variables in pp UPCs at $\sqrt{s_{NN}} = 7$ TeV.

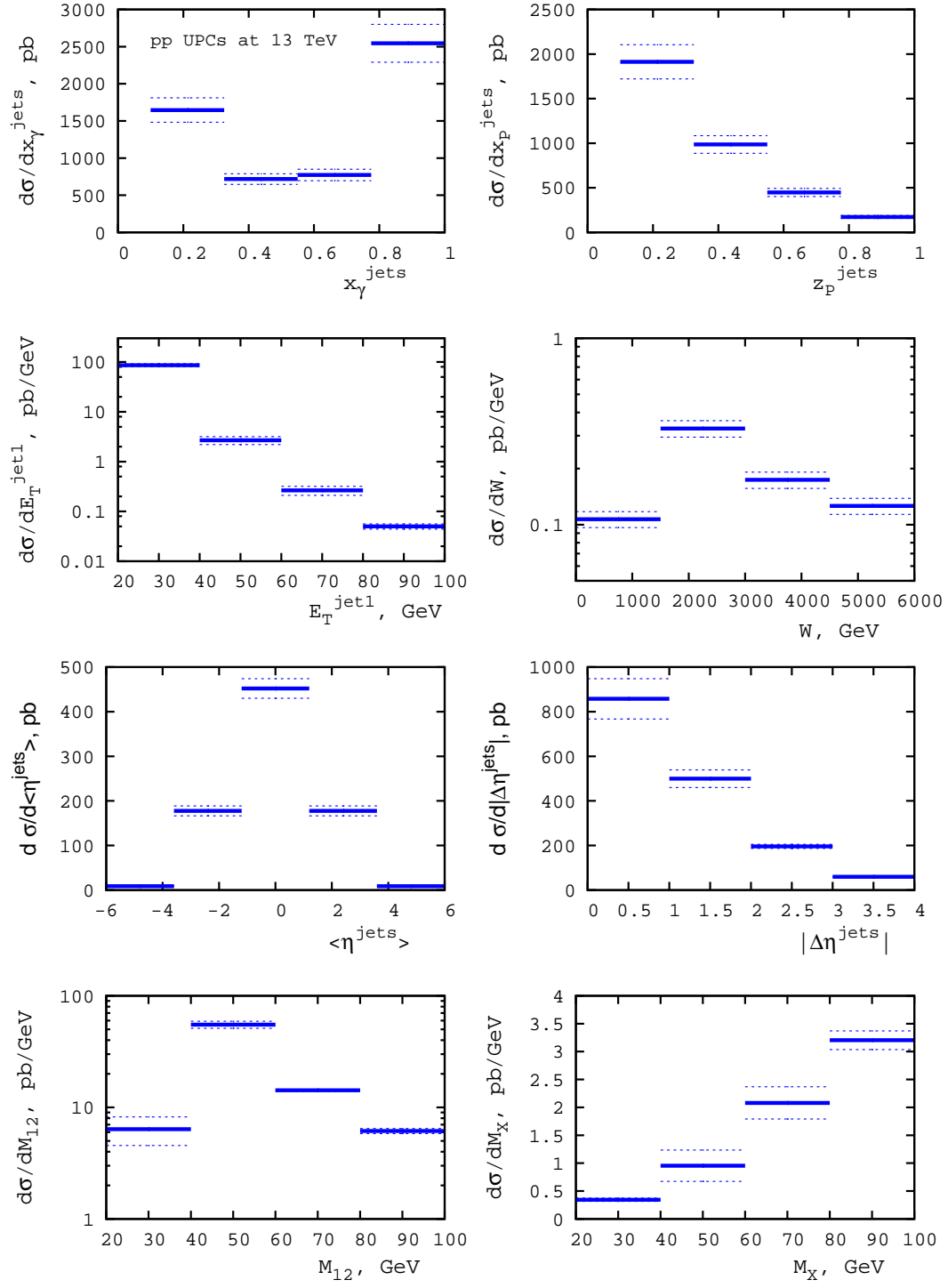


Figure 5. The same as in Fig. 4, but at $\sqrt{s_{NN}} = 13$ TeV.

3 Diffractive dijet photoproduction in proton–nucleus UPCs at the LHC

3.1 General expression for the cross section

Taking one of the ions in Fig. 1 to be a nucleus and the other one to be the proton, the cross section of diffractive dijet photoproduction in pA UPCs reads (see Eq. (2.1)):

$$d\sigma(pA \rightarrow p/A + 2\text{jets} + X' + Y) = d\sigma(pA \rightarrow A + 2\text{jets} + X' + Y)^{(+)} + d\sigma(pA \rightarrow p + 2\text{jets} + X' + Y)^{(-)}. \quad (3.1)$$

The first term in Eq. (3.1) corresponds to the process, when the photon flux is produced by the nucleus and the diffractive photoproduction of dijets takes place on the proton:

$$d\sigma(pA \rightarrow A + 2\text{jets} + X' + Y)^{(+)} = \sum_{a,b} \int_{t_{\text{cut}}}^{t_{\text{min}}} dt \int_{x_{\mathbb{P}}^{\text{min}}}^{x_{\mathbb{P}}^{\text{max}}} dx_{\mathbb{P}} \int_0^1 dz_{\mathbb{P}} \int_{y_{\text{min}}}^{y_{\text{max}}} dy \int_0^1 dx_{\gamma} \\ \times f_{\gamma/A}(y) f_{a/\gamma}(x_{\gamma}, \mu^2) f_{b/p}^{D(4)}(x_{\mathbb{P}}, z_{\mathbb{P}}, t, \mu^2) d\hat{\sigma}_{ab \rightarrow \text{jets}}^{(n)}. \quad (3.2)$$

Equation (3.2) is obtained from Eq. (2.3) by replacing the photon flux of the proton $f_{\gamma/p}(y)$ by the photon flux of the nucleus $f_{\gamma/A}(y)$ and effectively absorbing in it the factor of $S^2(y)$.

The second term in Eq. (3.1) corresponds to the process, when the photon flux is produced by the proton and the diffractive photoproduction of dijets takes place on the nucleus:

$$d\sigma(pA \rightarrow p + 2\text{jets} + X' + Y)^{(-)} = \sum_{a,b} \int_{t_{\text{cut}}}^{t_{\text{min}}} dt \int_{x_{\mathbb{P}}^{\text{min}}}^{x_{\mathbb{P}}^{\text{max}}} dx_{\mathbb{P}} \int_0^1 dz_{\mathbb{P}} \int_{y_{\text{min}}}^{y_{\text{max}}} dy \int_0^1 dx_{\gamma} \\ \times f_{\gamma/p}(y) f_{a/\gamma}(x_{\gamma}, \mu^2) f_{b/A}^{D(4)}(x_{\mathbb{P}}, z_{\mathbb{P}}, t, \mu^2) d\hat{\sigma}_{ab \rightarrow \text{jets}}^{(n)}, \quad (3.3)$$

where $f_{b/A}^{D(4)}$ is the diffractive PDF on a nucleus [55]; it is a novel, yet unmeasured distribution. Note that the photon flux $f_{\gamma/p}(y)$ in Eq. (3.3) corresponds to pA UPCs and includes the effect of the suppression of the strong photon–nucleus interaction at central impact parameters (see Sec. 3.2).

In Eqs. (3.2) and (3.3), the jet pseudorapidities η_1 and η_2 are defined with respect to the direction of the diffracting hadron. Therefore, $d\sigma(pA \rightarrow p + 2\text{jets} + X' + Y)^{(-)}$ is obtained from $d\sigma(pA \rightarrow A + 2\text{jets} + X' + Y)^{(+)}$ by the appropriate replacements of the photon flux and the diffractive PDFs as explained above and the inversion of the sign of η_1 and η_2 : $\eta_{1,2} \rightarrow -\eta_{1,2}$ (compare to Eq. (2.2)).

It is important to point out that for most of the observables or in the case of the integrated cross section, the pA UPC cross section Eq. (3.1) is dominated by the first term $d\sigma(pA \rightarrow A + 2\text{jets} + X' + Y)^{(+)}$. Indeed, while the photon flux of a nucleus scales as Z^2 , where Z is the nucleus charge, see, e.g. Eq. (2.10), the diffractive PDFs of a nucleus after integration over the momentum transfer t scale only as $A^{4/3}$ in the impulse approximation; they are also further suppressed by nuclear shadowing [55]. Therefore, pA UPCs can be used to primarily study diffractive photoproduction of dijets on the proton by taking advantage of the dramatically enhanced intensity of the photon flux compared to pp UPCs. The same situation arises in exclusive photoproduction of J/ψ mesons in pA UPCs at the LHC at $\sqrt{s_{NN}} = 5.02$ TeV [8].

3.2 Flux of equivalent photons in pA UPCs

To calculate the photon flux in pA UPCs, one needs to take into account the suppression of the strong interaction between the colliding proton and the nucleus. The resulting photon flux of the ultrarelativistic nucleus reads, see e.g. [56]:

$$f_{\gamma/A}(x) = \int d^2b \Gamma_{pA}(b) f_{\gamma/A}(x, b), \quad (3.4)$$

where b is the impact parameter (the transverse distance between the centers of mass of the nucleus and the proton); $\Gamma_{pA}(b)$ is the probability to not have the strong pA interaction at the impact parameter b ; and $f_{\gamma/A}(x, b)$ is the impact parameter dependent photon flux of the nucleus. The probability $\Gamma_{pA}(b)$ is given by the standard expression of the Glauber model for high-energy proton–nucleus scattering [57]:

$$\Gamma_{pA}(b) = e^{-\sigma_{NN}^{\text{tot}}(s)T_A(b)}, \quad (3.5)$$

where $\sigma_{NN}^{\text{tot}}(s)$ is the total nucleon–nucleon cross section; $T_A(b) = \int dz \rho_A(b, z)$ is the nuclear optical density, where ρ_A is the density of nucleons; and $\int d^2b T_A(b) = A$, where A is the atomic mass number. In our analysis, we use the fit of Ref. [51] for $\sigma_{NN}^{\text{tot}}(s)$, the two-parameter Fermi model parametrization for $\rho_A(b, z)$ [58], and Eq. (2.7) for $f_{\gamma/A}(x, b)$.

Figure 6 (left) shows the photon flux of Pb in pA UPCs at $\sqrt{s_{NN}} = 5.02$ TeV as a function of the photon momentum fraction x . The red solid curve labeled “FF+sup” corresponds to Eqs. (3.4) and (3.5); the blue dot-dashed curve labeled “FF” corresponds to the calculation when one sets $\Gamma_{pA}(b) = 1$.

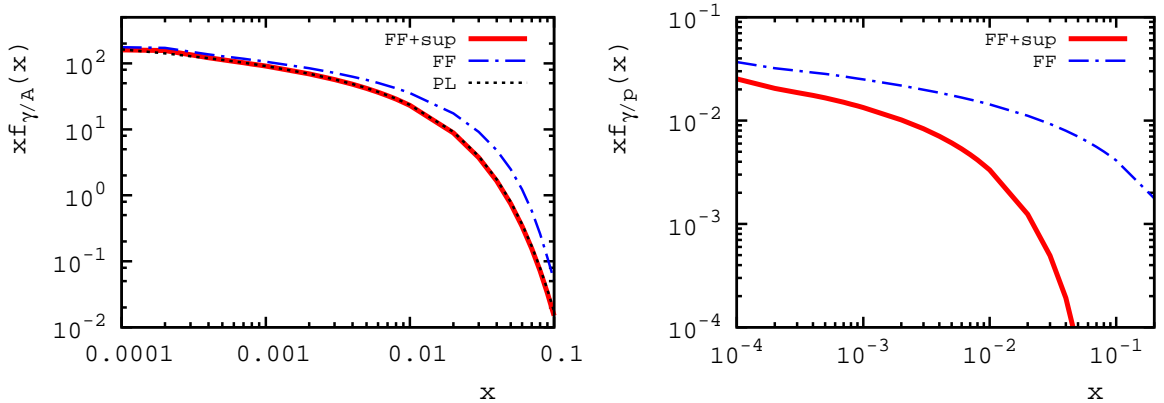


Figure 6. Left: The photon spectrum $x f_{\gamma/A}(x)$ of Pb in pA UPCs at $\sqrt{s_{NN}} = 5.02$ TeV as a function of the photon momentum fraction x . The red solid curve (“FF+sup”) is calculated using Eqs. (3.4) and (3.5); the blue dot-dashed curve (“FF”) corresponds to setting $\Gamma_{pA}(b) = 1$ in Eq. (3.4); the dotted curve (“PL”) is the flux of a point-like charge, Eq. (2.10), with $b_{\min} = 1.15R_A$. Right: The photon spectrum $x f_{\gamma/p}(x)$ of the proton in pA UPCs. For the labels, see the left panel and text.

In practice, the result of the full calculation can be approximated very well (with a few percent accuracy) by the photon flux of a point-like charge Eq. (2.10) with $b_{\min} = 1.15R_A$,

where $R_A = 1.145A^{1/3} \approx 6.8$ fm is the equivalent sharp radius of ^{208}Pb . The corresponding flux is given by the dotted curve labeled “PL”, which is indistinguishable from the red solid curve. Note that since $\Gamma_{pA}(b)$ is a slow function of s_{NN} in the considered energy range, it is a good approximation to use $b_{\min} = 1.15R_A$ both at $\sqrt{s_{NN}} = 5.02$ TeV and $\sqrt{s_{NN}} = 8.16$ TeV, the tentative Run-2 energy of pA collisions at the LHC.

The photon flux of the proton in pA UPCs can be found using Eq. (3.4), where one replaces $f_{\gamma/A}(x, b)$ by $f_{\gamma/p}(x, b)$. The result is shown by the red solid curve labeled “FF+sup” in the right panel of Fig. 6. For comparison, the blue dot-dashed curve labeled “FF” shows the result, when one sets $\Gamma_{pA} = 1$. Note that this curve coincides with the “DZ” and “PL” curves of Fig. 2 to a few percent accuracy. For convenience, in the Appendix we give a simple analytic form of the factor of $f_p^{\text{sup}}(x)$ parametrizing the difference between the “FF+sup” and “FF” curves shown in the right panel of Fig. 6. Note that $f_p^{\text{sup}}(x)$ does not change when one increases $\sqrt{s_{NN}}$ from $\sqrt{s_{NN}} = 5.02$ TeV to $\sqrt{s_{NN}} = 8.16$ TeV to better than a fraction of a percent accuracy.

One can readily see from Fig. 6 that $f_{\gamma/A}(x)$ is larger than $f_{\gamma/p}(x)$ by approximately a factor of 5,000 due to the Z^2 factor in Eq. (2.7). This enhancement of the $d\sigma(pA \rightarrow A + 2\text{jets} + X' + Y)^{(+)}$ term in Eq. (3.2) wins over the nuclear enhancement of nuclear diffractive PDFs (see below) entering the $d\sigma(pA \rightarrow p + 2\text{jets} + X' + Y)^{(-)}$ term. As a result, the process, when the photon flux is produced by the nucleus, dominates the cross section of pA UPCs unless one probes very large values of W and $\langle \eta^{\text{jets}} \rangle$ (see the results and discussion in Sec. 3.4).

3.3 Nuclear diffractive PDFs

The nuclear diffractive PDFs $f_{b/A}^{D(4)}(x_{\mathbb{P}}, z_{\mathbb{P}}, t, \mu^2)$ entering the $d\sigma(pA \rightarrow p + 2\text{jets} + X' + Y)^{(-)}$ term in Eq. (3.2) are conditional leading twist PDFs giving the distribution of a parton b in a nucleus in terms of the light-cone momentum fraction $z_{\mathbb{P}}$ at the resolution scale μ , provided that the nucleus undergoes diffractive scattering characterized by the light-cone momentum fraction loss $x_{\mathbb{P}}$ and the invariant momentum transfer squared t .

In the impulse approximation (IA), when the only nuclear effect is nuclear coherence, $f_{b/A}^{D(4)}(x_{\mathbb{P}}, z_{\mathbb{P}}, t, \mu^2)$ reads:

$$f_{b/A}^{D(4),\text{IA}}(x_{\mathbb{P}}, z_{\mathbb{P}}, t, \mu^2) = A^2 F_A^2(t) f_{b/p}^{D(4)}(x_{\mathbb{P}}, z_{\mathbb{P}}, t_{\min}, \mu^2), \quad (3.6)$$

where $F_A(t)$ is the nuclear form factor and $t_{\min} = -(x_{\mathbb{P}} m_p)^2 / (1 - x_{\mathbb{P}})$ is the minimal momentum transfer.

At high energies, the hard probe interacts coherently (simultaneously) with all nucleons of a nuclear target, which results in the effect of nuclear shadowing reducing nuclear PDFs compared to their IA expressions. In particular, the model of leading twist nuclear shadowing predicts a very significant suppression of nuclear diffractive PDFs [55], which can be quantified by the suppression factor of $R_b(x_{\mathbb{P}}, z_{\mathbb{P}}, \mu^2)$:

$$f_{b/A}^{D(4)}(x_{\mathbb{P}}, z_{\mathbb{P}}, t, \mu^2) = R_b(x_{\mathbb{P}}, z_{\mathbb{P}}, \mu^2) f_{b/A}^{D(4),\text{IA}}(x_{\mathbb{P}}, z_{\mathbb{P}}, t, \mu^2). \quad (3.7)$$

Note that nuclear shadowing of nuclear diffractive PDFs breaks the phenomenological factorization Eq. (2.4) of diffractive PDFs into the product of the “Pomeron” flux and PDFs of the “Pomeron”.

Predictions for $R_b(x_P, z_P, \mu^2)$ [55] for sea quarks for the representative ranges of z_P and x_P and at $\mu^2 = 400 \text{ GeV}^2$ are shown in Fig. 7. An analysis reveals that $R_b(x_P, z_P, \mu^2)$ very weakly depends on the parton flavor b , the scale μ , z_P and x_P (the latter is seen from Fig. 7). Therefore, in practical estimates, it is a good approximation to use the constant suppression factor:

$$R_b(x_P, z_P, \mu^2) \approx 0.15. \quad (3.8)$$

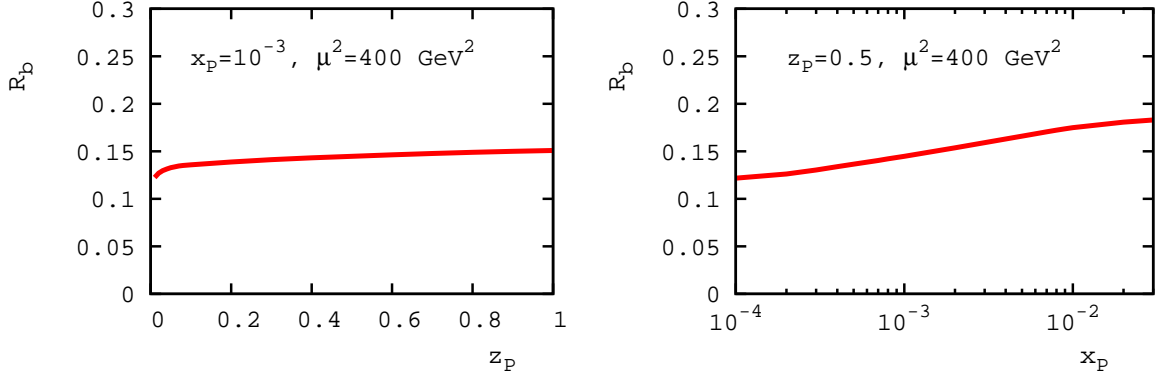


Figure 7. The suppression factor of $R_b(x_P, z_P, \mu^2)$, Eq. (3.7), quantifying the effect of nuclear shadowing of nuclear diffractive PDFs.

3.4 Results

We performed NLO calculations of the cross section of diffractive photoproduction of dijets in pA UPCs at $\sqrt{s_{NN}} = 5.02 \text{ TeV}$ and $\sqrt{s_{NN}} = 8.16 \text{ TeV}$ using the cuts of Eq. (2.16). The results are presented in Figs. 8 and 9, respectively.

In these figures, the blue solid and dotted lines give the net result of Eq. (3.1); the red dot-dashed lines show the contribution of the second term $d\sigma(pA \rightarrow p + 2\text{jets} + X' + Y)^{(-)}$ in Eq. (3.1) corresponding to the photon flux emitted by the proton. The blue solid and red dot-dashed lines correspond to $\mu = E_T^{\text{jet1}}$; the two blue dotted lines surrounding each solid line correspond to $\mu = 2E_T^{\text{jet1}}$ and $\mu = E_T^{\text{jet1}}/2$, respectively, which demonstrates the theoretical uncertainty of our predictions associated with the choice of the renormalization and factorization scale. One can see from the figures that this uncertainty is not significant.

A comparison of our predictions for pA UPCs shown in Figs. 8 and 9 to those for pp UPCs shown in Figs. 4 and 5 demonstrates that the general trends for the dependence of the cross section on various variables are similar in the pp and pA cases: very roughly, the pA results can be obtained from the pp ones by multiplying them by the scaling factor of $(1/2)Z^2(0.7 \text{ fm}/R_A) \approx 350$, where took into account that the photon spectra of the proton and a nucleus extend up to $x \sim 1/b_{\min} = 1/(0.7 \text{ fm})$ and $b_{\min} \sim 1/R_A$, respectively,

and that in the pA UPC cross section, the contribution of the minus-term in Eq. (3.1) is generally small. Note that in the two upper panels of Figs. 8 and 9, the physical units along the y -axis are nb.

At the same time, there are marked differences between the pA and pp results. First, the cross section falls off faster as one increases E_T^{jet1} or W in the pA case than in the pp case because the photon flux of a heavy ultrarelativistic nucleus decreases with an increase of the photon energy much faster than the photon flux of the proton. This also explains why at large values of E_T^{jet1} and W , the cross section is dominated by the photon-from-proton contribution (the term $d\sigma(pA \rightarrow p + 2\text{jets} + X' + Y)^{(-)}$ in Eq. (3.1) corresponding to the photon flux emitted by the proton).

Second, unlike the symmetric $\langle\eta^{\text{jets}}\rangle$ distribution in pp UPCs, this distribution is not symmetric in the case of pA UPCs. Indeed, at central and backward dijet rapidities, the dominant contribution to the cross section in Eq. (3.1) comes from low-energy photons emitted by the nucleus. At the same time, forward dijet rapidities correspond to high-energy photons emitted by the nucleus, where the photon flux is very small, or to low-energy photons emitted by the proton; the latter contribution dominates the cross section for sufficiently large positive $\langle\eta^{\text{jets}}\rangle$.

Note that without the effect of nuclear shadowing in nuclear diffractive PDFs, the photon-from-proton contribution (the red dot-dashed curves in Figs. 8 and 9) would be globally larger by a factor of $1/0.15 \approx 7$ (cf. Eq. (3.8)), with a weak dependence on $z_{\mathbb{P}}$ and $x_{\mathbb{P}}$ (cf. Fig. 7).

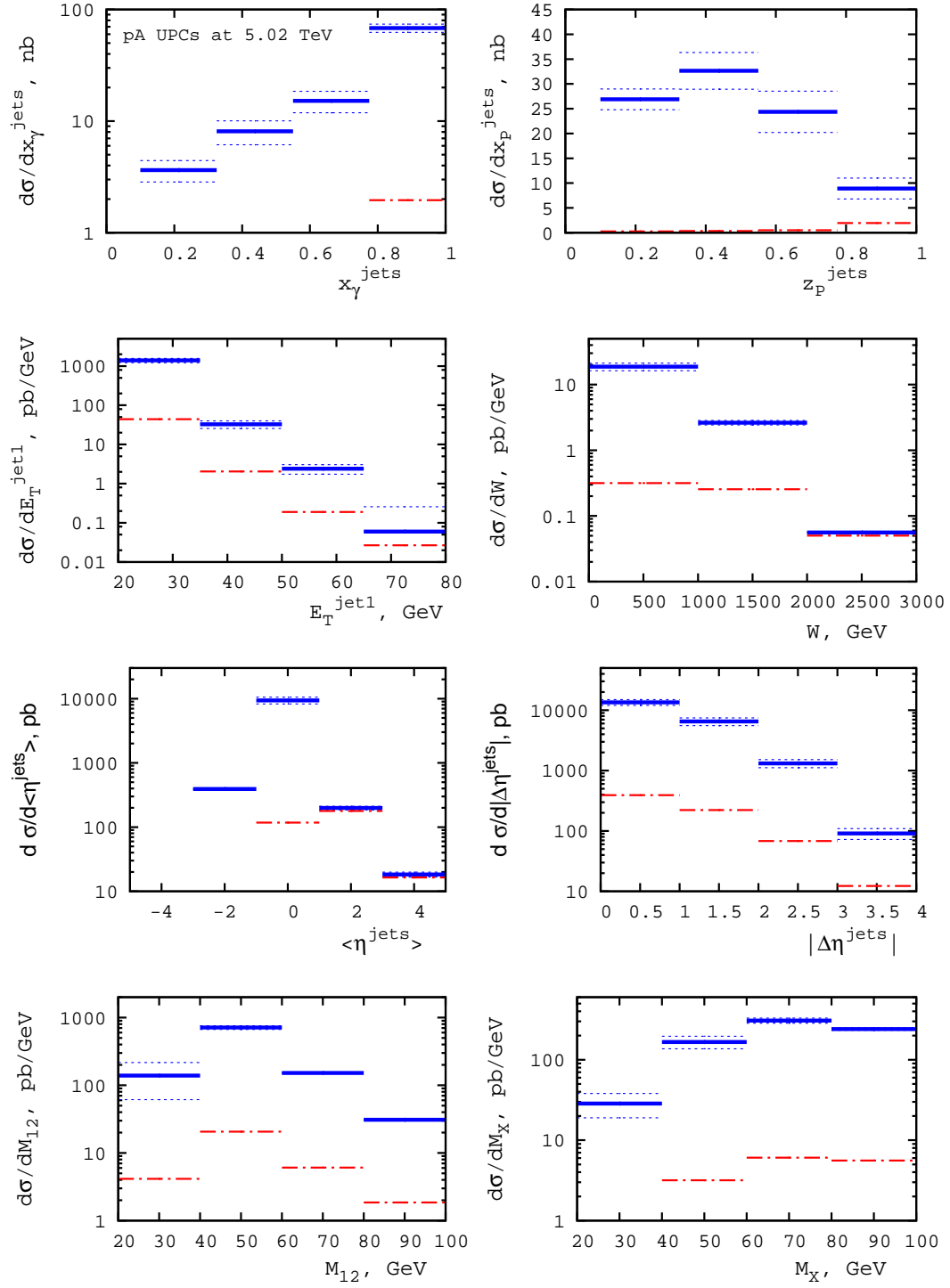


Figure 8. The differential cross section of diffractive photoproduction of dijets $d\sigma(pA \rightarrow p/A + 2\text{jets} + X' + Y)$ in pA UPCs at $\sqrt{s_{NN}} = 5.02$ TeV. The net result of Eq. (3.1) (blue solid and dotted lines) and the photon-from-proton contribution only (red dot-dashed lines) are shown separately.

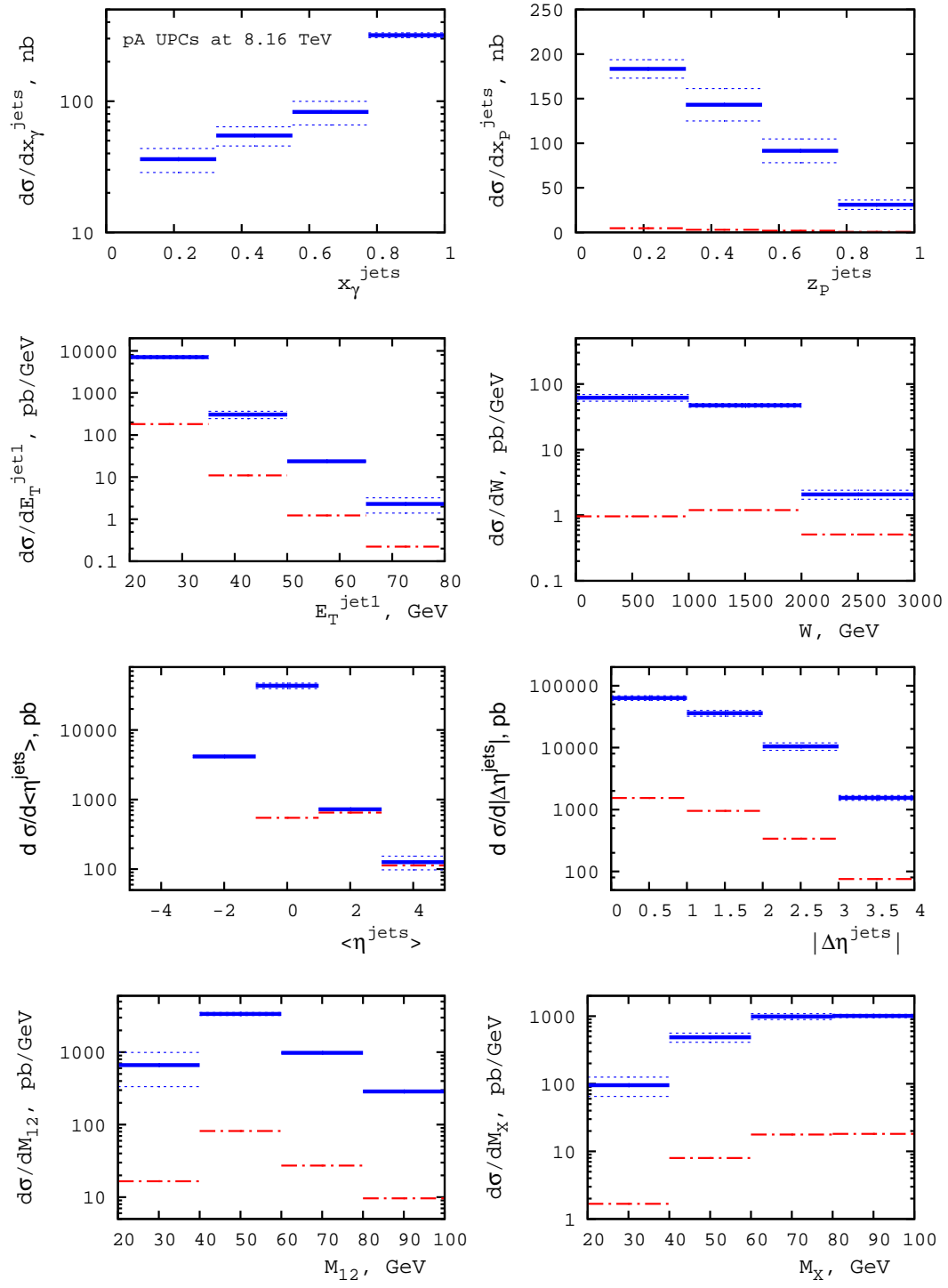


Figure 9. The same as in Fig. 8, but at $\sqrt{s_{NN}} = 8.16$ TeV.

4 Diffractive dijet photoproduction in nucleus–nucleus UPCs at the LHC

4.1 General expression for the cross section

Considering nucleus–nucleus UPCs, we can readily write down the cross section of coherent diffractive dijet photoproduction (compare to Eqs. (2.1) and (3.1)):

$$d\sigma(AA \rightarrow A + 2\text{jets} + X' + A) = d\sigma(AA \rightarrow A + 2\text{jets} + X' + A)^{(+)} + d\sigma(AA \rightarrow A + 2\text{jets} + X' + A)^{(-)}. \quad (4.1)$$

Note that we considered the case of coherent nuclear scattering when both nuclei remain intact after either the photon emission or hard dijet photoproduction.

By analogy with the pp and pA cases considered above, each term in Eq. (4.1) can be written as a convolution of the photon flux of an ultrarelativistic nucleus $f_{\gamma/A}(y)$, the PDF of the photon $f_{a/\gamma}$, the nuclear diffractive PDFs $f_{b/A}^{D(4)}$, and the hard elementary cross section $d\hat{\sigma}_{ab \rightarrow \text{jets}}^{(n)}$, see Eqs. (2.3), (3.2) and (3.3). For instance, one obtains for the first term:

$$d\sigma(AA \rightarrow A + 2\text{jets} + X' + A)^{(+)} = \sum_{a,b} \int_{t_{\text{cut}}}^{t_{\text{min}}} dt \int_{x_{\mathbb{P}}^{\text{min}}}^{x_{\mathbb{P}}^{\text{max}}} dx_{\mathbb{P}} \int_0^1 dz_{\mathbb{P}} \int_{y_{\text{min}}}^{y_{\text{max}}} dy \int_0^1 dx_{\gamma} \\ \times f_{\gamma/A}(y) f_{a/\gamma}(x_{\gamma}, \mu^2) f_{b/A}^{D(4)}(x_{\mathbb{P}}, z_{\mathbb{P}}, t, \mu^2) d\hat{\sigma}_{ab \rightarrow \text{jets}}^{(n)}. \quad (4.2)$$

For symmetric (equal beam-energy) AA UPCs that we consider in our work, the second and first terms in Eq. (4.1) are related by a sign exchange of the dijet rapidities:

$$d\sigma(AA \rightarrow A + 2\text{jets} + X' + A)^{(-)} = d\sigma(AA \rightarrow A + 2\text{jets} + X' + A)^{(+)}_{|\eta_1 \rightarrow -\eta_1, \eta_2 \rightarrow -\eta_2}. \quad (4.3)$$

4.2 Flux of equivalent photons in AA UPCs

In the calculation of the photon flux produced by each ultrarelativistic nucleus in AA UPCs, one needs to suppress the strong nucleus–nucleus interaction. The resulting expression for the photon flux $f_{\gamma/A}(x)$ is

$$f_{\gamma/A}(x) = \int d^2b \Gamma_{AA}(b) f_{\gamma/A}(x, b), \quad (4.4)$$

where $f_{\gamma/A}(x, b)$ is the impact parameter dependent photon flux of the nucleus (2.7) and $\Gamma_{AA}(b)$ is the probability for the nuclei to not interact strongly at the impact parameter b . It is given by the standard expression of the Glauber model for high-energy nucleus–nucleus scattering:

$$\Gamma_{AA}(b) = \exp \left(-\sigma_{NN}^{\text{tot}}(s) \int d^2\vec{b}_1 T_A(\vec{b}) T_A(\vec{b}_1 - \vec{b}) \right). \quad (4.5)$$

An analysis shows that the result of the calculation of the photon flux using the exact expression of Eq. (4.4) can be very well approximated by the much simpler expression for the photon flux produced by a relativistic point-like charge Z in Eq. (2.10), when one uses $b_{\text{min}} \approx 2R_A$ for the minimal impact parameter, where R_A is the equivalent sharp nucleus

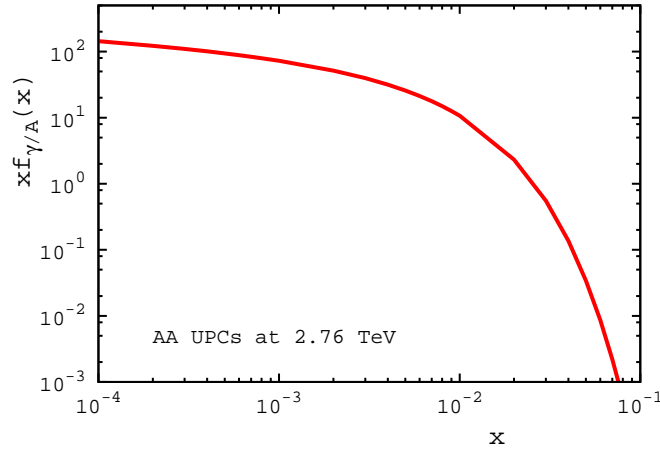


Figure 10. The photon spectrum $x f_{\gamma/A}(x)$ of Pb in AA UPCs at $\sqrt{s_{NN}} = 2.76$ TeV as a function of the photon momentum fraction x .

radius. Therefore, in our analysis of Pb-Pb UPCs at the LHC, we used Eq. (2.10) for the Pb photon flux in Eq. (4.2) with $b_{\min} \approx 2.1R_A = 14.2$ fm [49]. The resulting photon spectrum $x f_{\gamma/A}(x)$ as a function of the energy fraction x is shown in Fig. 10. Note that in our analysis we assume that $f_{\gamma/A}(x)$ does not change when one increases the invariant collision energy from $\sqrt{s_{NN}} = 2.76$ TeV to $\sqrt{s_{NN}} = 5.1$ TeV, the tentative Run-2 energy of AA collisions at the LHC.

4.3 Results

The results of our NLO calculations of the cross section of diffractive photoproduction of dijets in AA UPCs at $\sqrt{s_{NN}} = 2.76$ TeV and $\sqrt{s_{NN}} = 5.1$ TeV are presented in Figs. 11 and 12, respectively. In the calculations, we used the cuts of Eq. (2.16). As in the pp and pA cases, the blue solid lines correspond to the $\mu = E_T^{\text{jet1}}$ choice of the renormalization and factorization scale; the two dot-dashed lines surrounding the solid one correspond to $\mu = 2E_T^{\text{jet1}}$ and $\mu = E_T^{\text{jet1}}/2$ and, thus, illustrate the theoretical uncertainty of our calculations associated with the choice of the two scales.

One can see from these figures that the general trends of the dependence of the cross section of diffractive dijet photoproduction in AA UPCs resemble closely those already observed in the pp and pA and can be obtained approximately by simple rescaling. For instance, a comparison of the AA results at $\sqrt{s_{NN}} = 5.1$ TeV with the pA results at $\sqrt{s_{NN}} = 8.16$ TeV (corresponding to the same nucleus beam energy), one finds that the scaling factor between the distributions in the two cases is approximately A . In this estimate, we took into account that in the bulk of the considered kinematics, one has the approximate relation $f_{j/A}^{D(3)}(x_P, z_P, \mu^2) \approx A/2 f_{j/p}^{D(3)}(x_P, z_P, \mu^2)$ between the nucleus and proton diffractive PDFs, integrated over the momentum transfer t , (see Eqs. (3.6)–(3.8)), and that the AA UPC cross section receives contributions of both nuclei, while the pA UPC cross section is dominated by the photon-from-nucleus contribution.

Note that the strong nuclear shadowing suppresses nuclear diffractive PDFs by the factor of 0.15, see Eq. (3.8); without this effect, i.e., in the impulse approximation, our results in Figs. 11 and 12 would be increased approximately by the factor of seven.

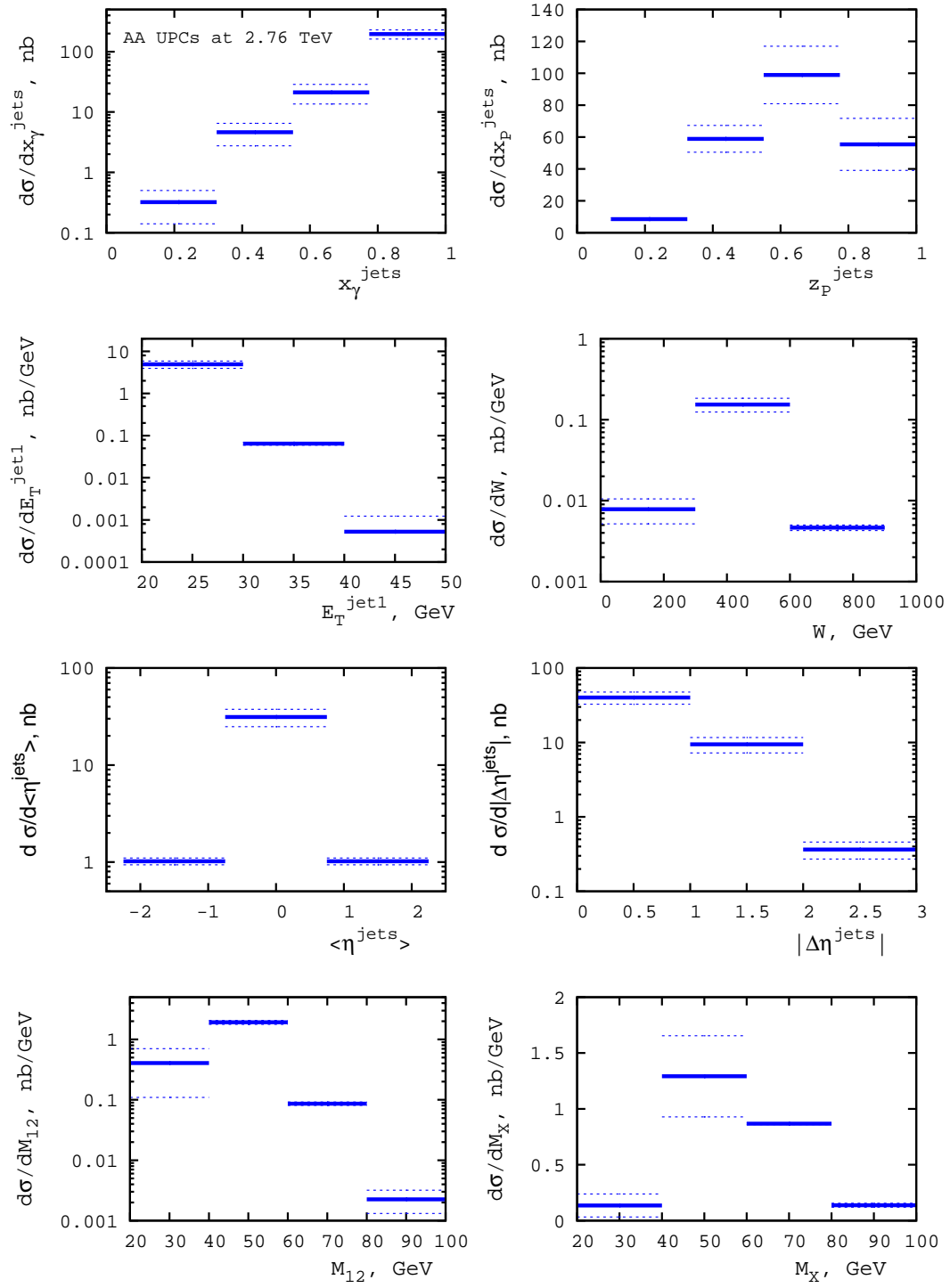


Figure 11. The differential cross section of diffractive photoproduction of dijets $d\sigma(AA \rightarrow A + 2\text{jets} + X' + A)$ in AA UPCs at $\sqrt{s_{NN}} = 2.76$ TeV.

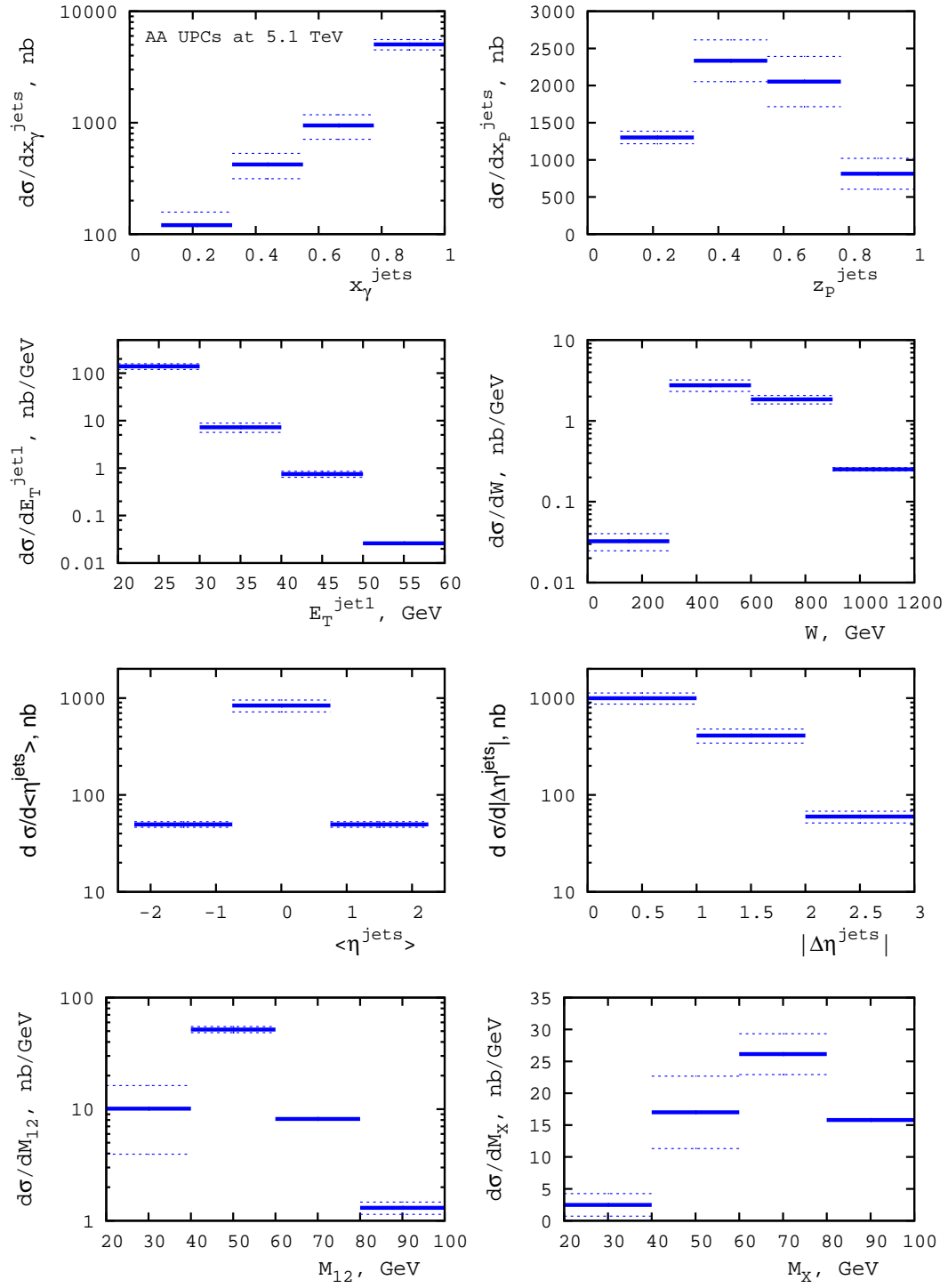


Figure 12. The same as Fig. 11, but at $\sqrt{s_{NN}} = 5.1$ TeV.

5 Factorization breaking in diffractive dijet photoproduction

It is well known from studies of diffractive photoproduction of dijets in ep scattering at HERA that collinear factorization for this process is broken, i.e., NLO pQCD calculations overestimate the measured cross sections by almost a factor of two [25–33]. However, the pattern of this factorization breaking remains unknown and presents one of the outstanding questions in this field: the data and the theory can be made consistent by introducing either the global suppression factor of $R(\text{glob.}) \approx 0.5$ or the suppression factor of $R(\text{res.}) \approx 0.4$ only for the resolved photon contribution.

In addition, the HERA data on diffractive photoproduction of open charm [59] are in agreement with NLO pQCD calculations, which is consistent with diffractive QCD factorization. This agreement can be interpreted as an indication of absence of factorization breaking for the direct photon contribution and the charm-quark part of the resolved photon contribution to the dijet photoproduction cross section. Hence, it challenges the global suppression scenario of diffractive factorization breaking.

Factorization breaking in diffractive dijet photoproduction results from soft inelastic photon interactions with the proton (nucleus), which populate and thus partially destroy the final-state rapidity gap. Thus, it has exactly the same nature as the rapidity gap survival probability S^2 , which we discussed above in relation to pp UPCs, see Eq. (2.12). At high energies, the photon interacts with protons and nuclei by fluctuating into various hadronic configurations (components) interacting with the target with different cross sections. Thus, it is natural to put forward the following physics scenario [60]: for the direct photon contribution, corresponding to weakly-interacting (point-like) fluctuations of the photon, factorization holds; for the resolved photon contribution corresponding to large-size photon fluctuations interacting with a typical vector meson–nucleon cross section, factorization is broken, which leads to the suppression factor of $R(\text{res.}) \approx 0.3 - 0.4$. Note that beyond the leading order of pQCD, the separations of the direct and resolved contributions is ambiguous and depends on the factorization scheme and the factorization scale [31, 37]; in the present work, we use the conventions of [33].

Our results presented so far in Figs. 4, 5, 8, 9, 11 and 12 assume no factorization breaking. Based on the observations and arguments summarized above, we will test the following two competing scenarios of diffractive QCD factorization breaking and implement them in our predictions for the cross section of diffractive dijet photoproduction: first, we assume the global suppression factor of $R(\text{glob.}) = 0.5$ for the proton target and $R(\text{glob.}) = 0.1$ for the nucleus target (the latter value is somewhat ad hoc, but reflects the important observation that it is much easier to break the nucleus than the proton, see Fig. 13 and its discussion below); second, we assume that the resolved photon contribution enters with the suppression factor of $R(\text{res.})$, while the direct photon contribution is unsuppressed. To estimate $R(\text{res.})$, we use the appropriate application of the two-state eikonal model of [50, 61] (compare to Eq. (2.12)):

$$R(\text{res.}) = \frac{\int d^2b |\mathcal{A}_{\gamma T \rightarrow VT}(W, b)|^2 P_{VT}(W, b)}{\int d^2b |\mathcal{A}_{\gamma T \rightarrow VT}(W, b)|^2}, \quad (5.1)$$

where T stands for the proton or nucleus target; V denotes the hadron-like fluctuation (component) of the photon, which is assumed to be represented by the ρ meson; $\mathcal{A}_{\gamma T \rightarrow VT}(W, b)$ is the $\gamma T \rightarrow VT$ amplitude in impact parameter space; $P_{VT}(W, b)$ is the probability to not have the strong inelastic vector meson–target interaction at the impact parameter b ; and W is the invariant photon–nucleon energy.

For the proton target, we use

$$|\mathcal{A}_{\gamma p \rightarrow Vp}(W, b)|^2 = e^{-b^2/B(W)} |\mathcal{A}_{\gamma p \rightarrow Vp}(W, b=0)|^2, \quad (5.2)$$

where $B(W)$ is the slope of the t -dependence of the $\gamma p \rightarrow \rho p$ cross section. A fit to the available HERA data gives $B(W) = [11 + 0.5 \ln(W/W_0)^2] \text{ GeV}^{-2}$, where $W_0 = 72 \text{ GeV}$ [62, 63].

For the probability $P_{Vp}(W, b)$, we use Eqs. (2.13) and (2.14), where in the expression for the proton optical density, we substitute the total proton–proton cross section $\sigma_{pp}^{\text{tot}}(s)$ by the ρ meson–nucleon cross section $\sigma_{\rho N}(W)$. Since we are interested in the large values of $W > 100 \text{ GeV}$ well beyond the HERA reach, we use in our analysis the following simple and conservative extrapolation:

$$\sigma_{\rho N}(W) = 26 \left(\frac{W^2}{W_0^2} \right)^{0.08} \text{ mb}, \quad (5.3)$$

where $W_0 = 100 \text{ GeV}$. The value of $\sigma_{\rho N}(W)$ at $W = 100 \text{ GeV}$ agrees with the analysis of Ref. [24].

To find $R(\text{res.})$ for the nuclear target, we calculate $\mathcal{A}_{\gamma A \rightarrow VA}(W, b)$ in Eq. (5.1) using the Glauber model of nuclear shadowing for coherent photoproduction of vector mesons on nuclei in the high-energy limit, see e.g. [64]:

$$\mathcal{A}_{\gamma A \rightarrow VA}(W, b) = \frac{e}{f_V} \left(1 - e^{-\frac{\sigma_{\rho N}(W)}{2} T_A(b)} \right), \quad (5.4)$$

where $T_A(b)$ is the nuclear optical density normalized to the number of nucleons A and $f_V^2/(4\pi) = 2.01$ is the photon– ρ meson coupling constant determined from the $\rho \rightarrow e^+e^-$ decay. Note that in Eq. (5.4) we neglected the effect of the inelastic (Gribov) nuclear shadowing — at the large values of W that we consider, due to an eventual decrease of the dispersion of hadronic fluctuations of a projectile with an increase of energy [65], the relative importance of inelastic nuclear shadowing in our case is much smaller than that in the case of coherent ρ and ϕ photoproduction in AA UPCs [24, 66].

For the suppression factor of $P_{VA}(W, b)$ in Eq. (5.1), we use the standard Glauber model expression for the probability to not have the strong inelastic resolved photon (ρ meson)–nucleus interaction at the impact parameter b (compare to Eq. (3.5)):

$$P_{VA}(W, b) = e^{-\sigma_{\rho N}(W) T_A(b)}. \quad (5.5)$$

Figure 13 shows the resulting values of $R(\text{res.})$ for the proton (left panel) and Pb (right panel) as a function of the invariant photon–nucleon energy W . One can see from the figure that for the proton, $R(\text{res.}) \approx 0.4$, which is in agreement with the original result of [50].

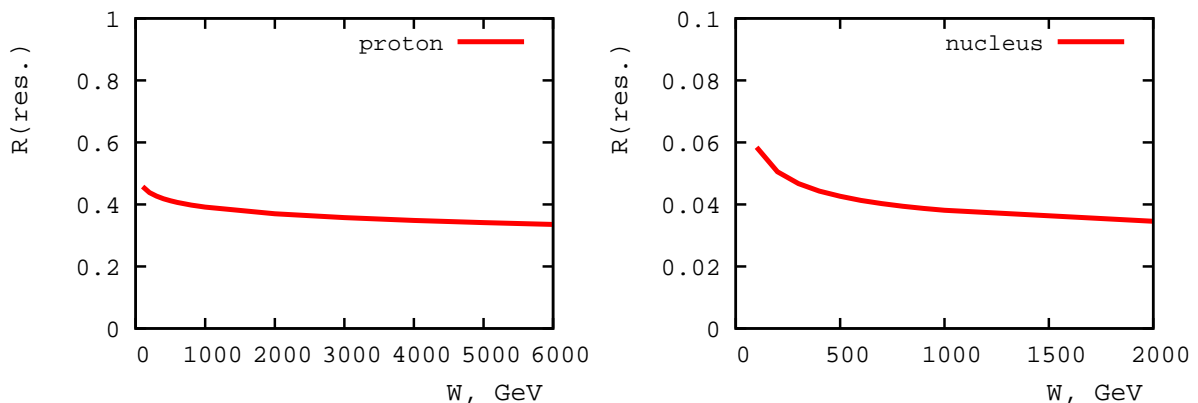


Figure 13. The factor of $R(\text{res.})$, Eq. (5.1), quantifying the effect of factorization breaking (suppression) for the resolved photon contribution.

For Pb, the values of $R(\text{res.})$ are an order of magnitude smaller, $R(\text{res.}) \approx 0.04$, which reflects the very small probability of rapidity gap events with nuclear targets.

While our second scenario involving $R(\text{res.})$ captures the bulk of physics of diffractive factorization breaking coming from the hadron structure of the photon, it neglects such subtle points as the possible dependence of $R(\text{res.})$ on the parton flavor and x_γ due to the separation of the resolved contribution into the point-like and hadronic terms, the hadronization corrections and bin migration effects, see the discussion in Ref. [60]. Our aim here is to examine whether studies of diffractive dijet photoproduction in UPCs can help to distinguish between the two scenarios and, thus, to complement and extend the analysis of this process at HERA.

Note that for the first time, the issue of nuclear dependence of factorization breaking in diffractive dijet production in hard and ultraperipheral pA scattering was considered in [67]. It was found that soft inelastic proton–nucleus interactions significantly suppress the rapidity gap probability in hard pA scattering, which is in line with the small values of $R(\text{glob.})$ and $R(\text{res.})$ for the nucleus target, which we use in our analysis.

The resulting cross sections of diffractive dijet photoproduction in pp , pA and AA UPC are presented in Fig. 14–19. The red solid lines correspond to the global suppression factor of $R(\text{glob.}) = 0.5$ for the proton target and $R(\text{glob.}) = 0.1$ for the nucleus target (note that in the case of pA UPCs, we encounter a mixed situation); the blue dot-dashed lines correspond to the suppression of the resolved photon contribution only: $R(\text{res.}) = 0.4$ for the diffracting proton (pp and the photon-from-nucleus contribution to pA) and $R(\text{res.}) = 0.04$ for the diffracting nucleus (the photon-from-proton contribution to pA and AA). For comparison, we also show our results that do not include the effect of diffractive QCD factorization breaking by black dotted lines labeled “ $R = 1$ ”. Note that in all cases, we show only the predictions corresponding to the central value of the renormalization and factorization scale $\mu = E_T^{\text{jet}1}$.

As one observes, the most sensitive variable to distinguish global from resolved-only

suppression is x_γ^{jets} as expected, where resolved-only suppression is smaller in the highest and larger in the lower bins. As also observed previously in diffractive dijet photoproduction at HERA [31], the distributions in E_T^{jet1} also show differences, i.e. resolved-only suppression results in harder spectra than global suppression. These differences are more pronounced in pA collisions compared to pp collisions due to the enhanced photon flux and asymmetric experimental setup. In pA UPCs, also the z_P^{jets} distributions differ, i.e. resolved-only suppression is less effective at small values of that variable, which are correlated with large x_γ^{jets} . Naturally, similar differences are then observed in the average rapidity and rapidity difference distributions, from which the observed momentum fraction variables are derived. In pA UPCs, the differences of the two suppression schemes are furthermore enhanced at higher center-of-mass energy, where the low z_P^{jets} region is particularly enhanced. In contrast, in AA collisions the shape of the z_P distribution is quite different from those in pp and pA collisions, but is similar in the two used suppression schemes, which makes it less sensitive to the factorization breaking pattern.

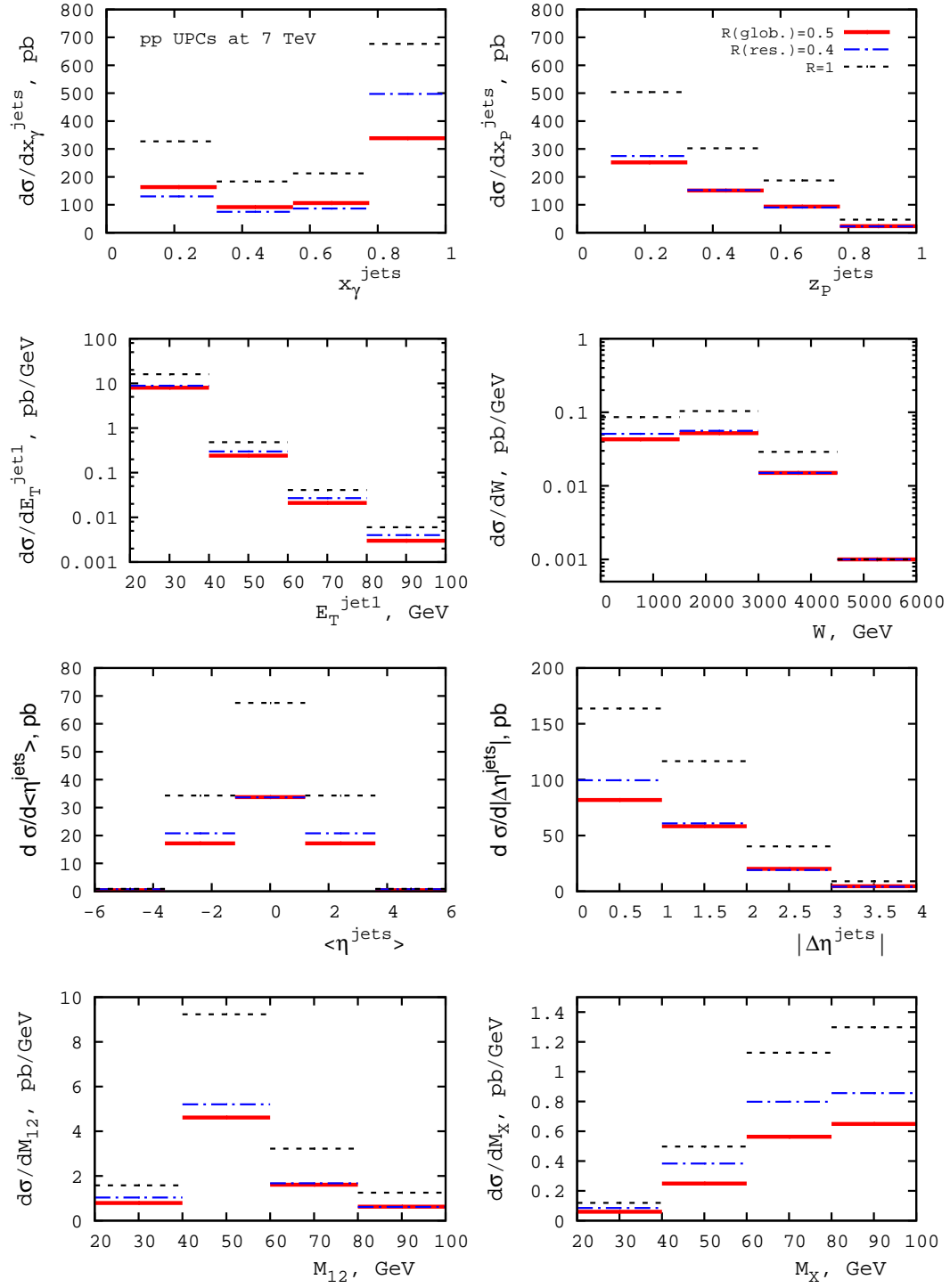


Figure 14. The effect of diffractive factorization breaking on the differential cross section of diffractive photoproduction of dijets $d\sigma(pp \rightarrow p + 2\text{jets} + X' + Y)$ in pp UPCs at $\sqrt{s_{NN}} = 7$ TeV.

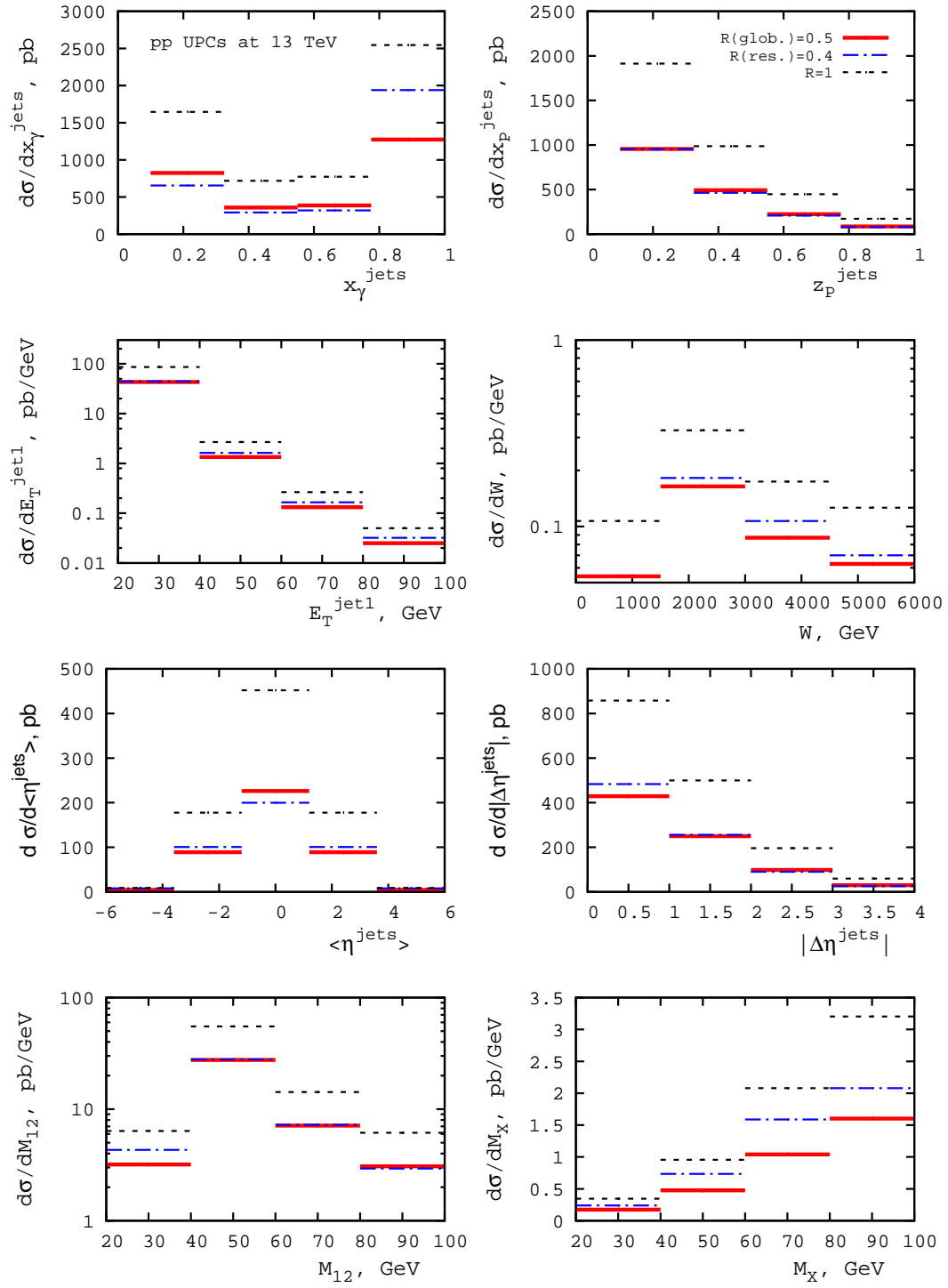


Figure 15. The same as in Fig. 14, but at $\sqrt{s_{NN}} = 13$ TeV.

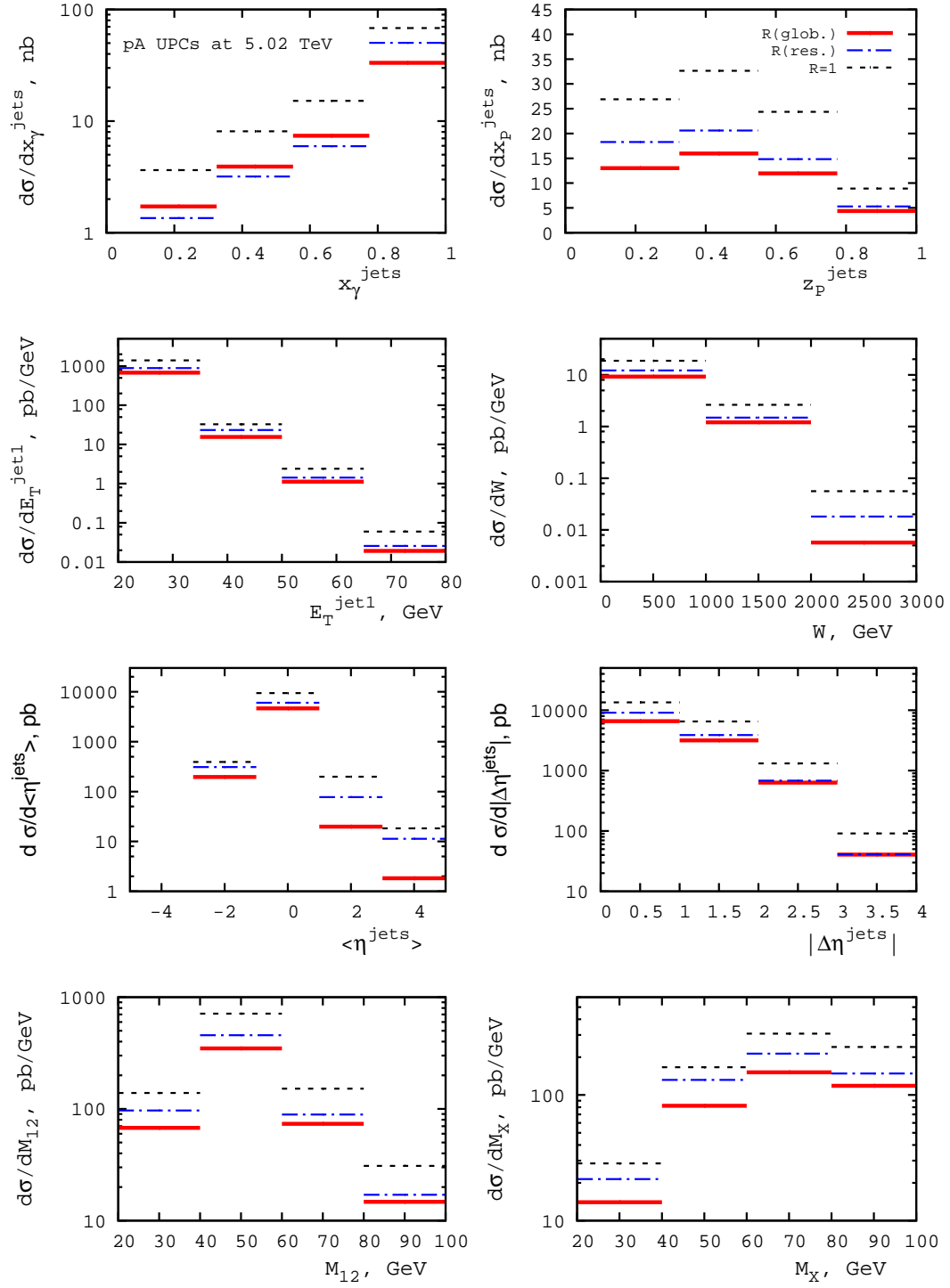


Figure 16. The effect of diffractive factorization breaking on the cross section of diffractive photoproduction of dijets $d\sigma(pA \rightarrow p/A + 2\text{jets} + X' + Y)$ in pA UPCs at $\sqrt{s_{NN}} = 5.02$ TeV.

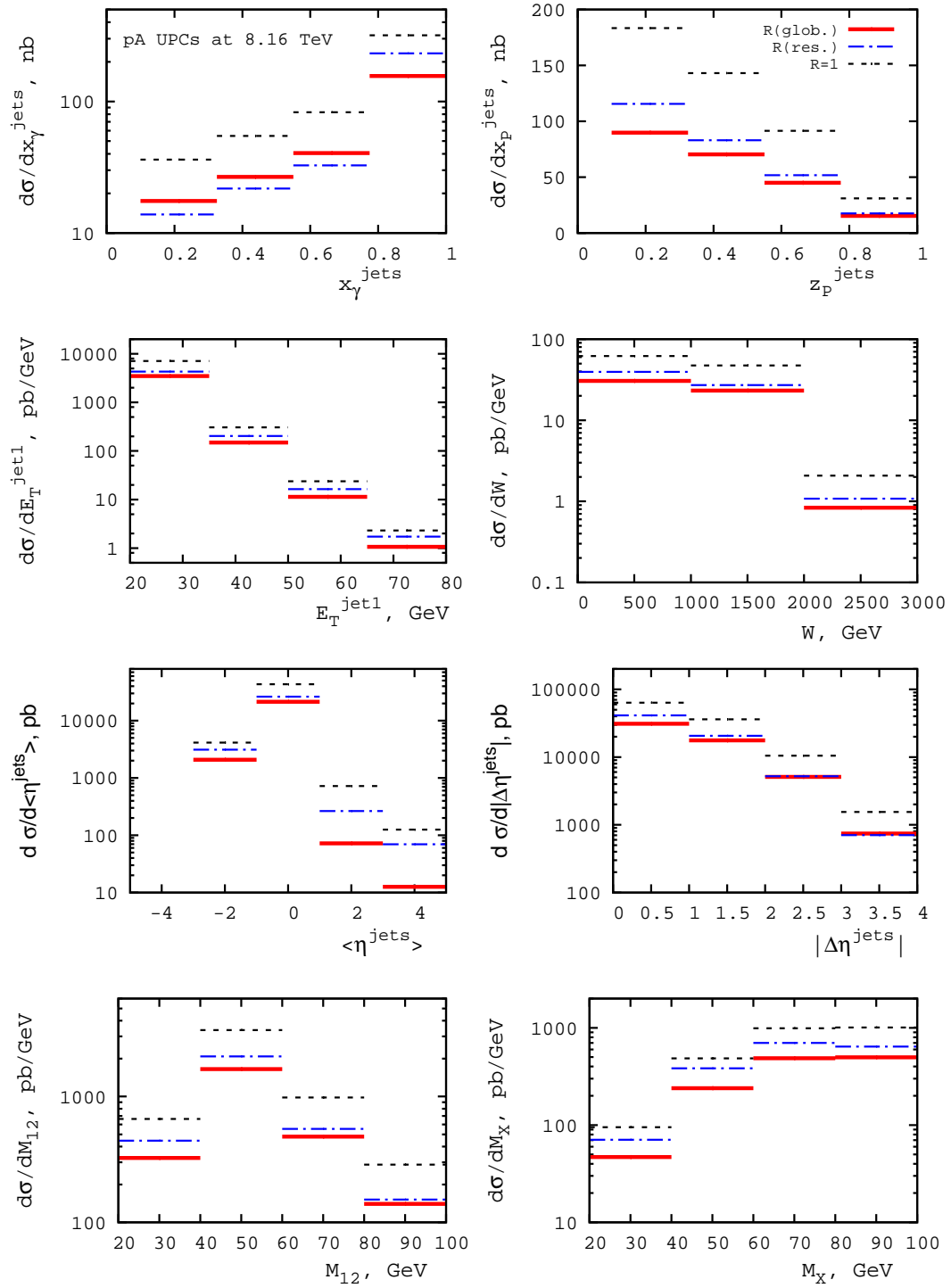


Figure 17. The same as in Fig. 16, but at $\sqrt{s_{NN}} = 8.16$ TeV.

6 Conclusions

For the first time, using NLO pQCD, we make predictions for the cross sections of diffractive dijet photoproduction in pp , pA and AA UPCs in the kinematics of Runs 1 and 2 at the

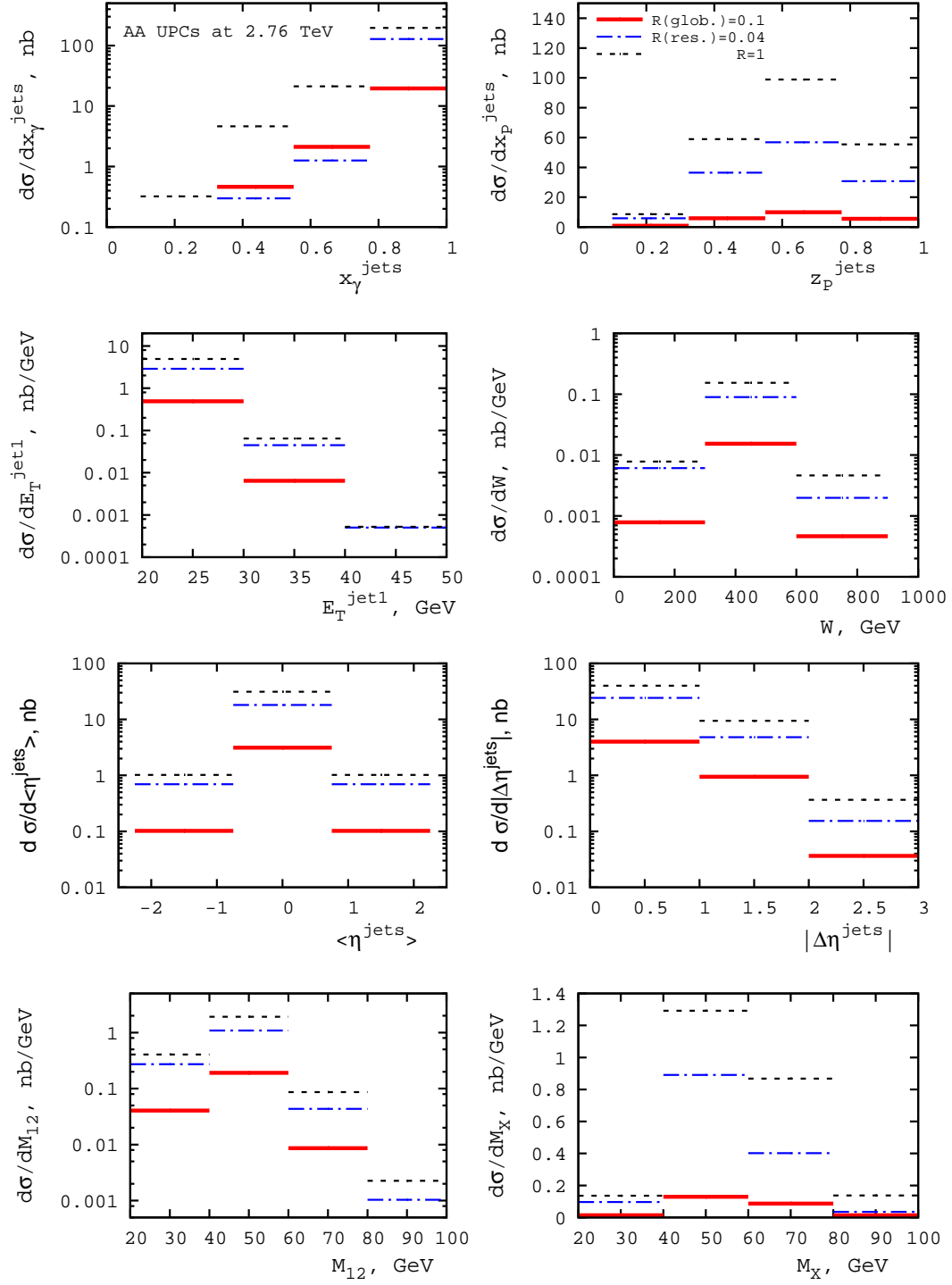


Figure 18. The effect of diffractive factorization breaking on the differential cross section of diffractive photoproduction of dijets $d\sigma(AA \rightarrow A + 2\text{jets} + X' + A)$ in AA UPCs at $\sqrt{s_{NN}} = 2.76$ TeV.

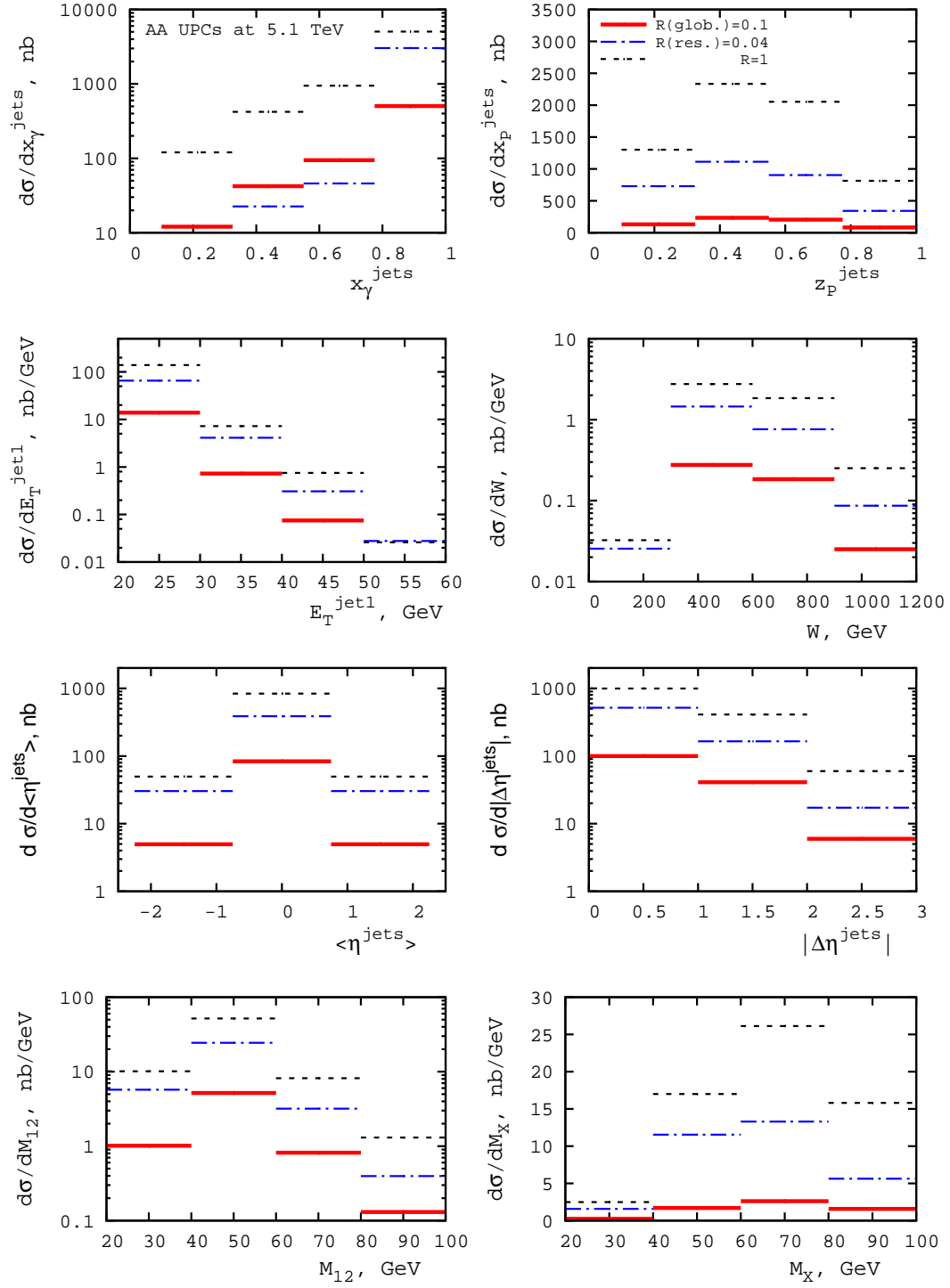


Figure 19. The same as Fig. 18, but at $\sqrt{s_{NN}} = 5.1$ TeV.

LHC. Using general kinematic conditions and cuts on the final state, we found that the

values of the cross section as a function of various variables are sufficiently large, i.e., this process can be observed. Compared to studies of this process in ep scattering at HERA, we observe that UPCs provide an enhanced sensitivity to the low- $z_{\mathcal{P}}^{\text{jets}}$ region probing the quark and gluon diffractive parton distributions in the proton and nuclei at small momentum fractions z and an access to much larger values of W .

In our calculations, we used nuclear diffractive PDFs, which are strongly suppressed by nuclear shadowing; neglecting this effect, our predictions for AA UPCs and for the photon–nucleus contribution to pA UPCs would be larger by the factor of seven.

UPCs also give a new handle on the issue of diffractive QCD factorization breaking through its A dependence: while the two competing schemes of factorization breaking based on the global and resolved-only suppression factors give rather similar predictions for pp UPCs (like in the case of ep scattering at HERA), the two scenarios give rather different predictions for AA UPCs and to some extent for pA UPCs. The best observable to look for this effect is the x_{γ}^{jets} dependence at large x_{γ}^{jets} , which is dominated by the direct photon contribution and where the ordering between the cross sections calculated using $R(\text{glob.})$ and $R(\text{res.})$ changes. This is illustrated in Fig. 20 summarizing our results for the x_{γ}^{jets} dependence in Run 1 (upper panel) and Run 2 (lower panel). Note that in this figure, the two schemes of factorization breaking for the pp case are indistinguishable.

The results presented in this work are based on the NLO collinear factorization formalism of pQCD. In the framework of high-energy QCD, diffractive dijet production in photon–proton and photon–nucleus collisions was considered in the Color Glass Condensate (CGC) formalism at leading order in Ref. [68]. It was found that the effects of gluon saturation can be searched for in the dijet azimuthal angle correlations and t distributions. In addition, a theoretical framework for diffractive production of jets in the QCD shock-wave approach has started to be developed in a series of papers [69, 70]. It will be interesting to confront these different approaches with LHC data in the future.

A Suppression factors used for calculations in this paper

For convenience of the reader, we give in this Appendix simple parametrizations of the various suppression factors used in our calculations in this paper.

1. The rapidity gap survival probability factor of $S^2(x)$ for pp UPCs, which is given by Eq. (2.12) and shown in Fig. 3, can be fitted to better than 5% accuracy by the following simple form:

$$S^2(x) = \frac{0.85}{1 + ax + bx^2}, \quad (\text{A.1})$$

where $a = 14$ and $b = 1.4$ at $\sqrt{s_{NN}} = 7$ TeV; $a = 15$ and $b = 4.8$ at $\sqrt{s_{NN}} = 13$ TeV.

2. To quantify the suppression of the photon flux of the proton in pA UPCs due to the strong interaction, it is convenient to introduce the factor of $f_p^{\text{sup}}(x)$ (see Eqs. (3.4) and (3.5)):

$$f_p^{\text{sup}}(x) \equiv \frac{\int d^2b \Gamma_{pA}(b) f_{\gamma/p}(x, b)}{f_{\gamma/p}(x)} = \frac{0.71}{1 + 260x}. \quad (\text{A.2})$$

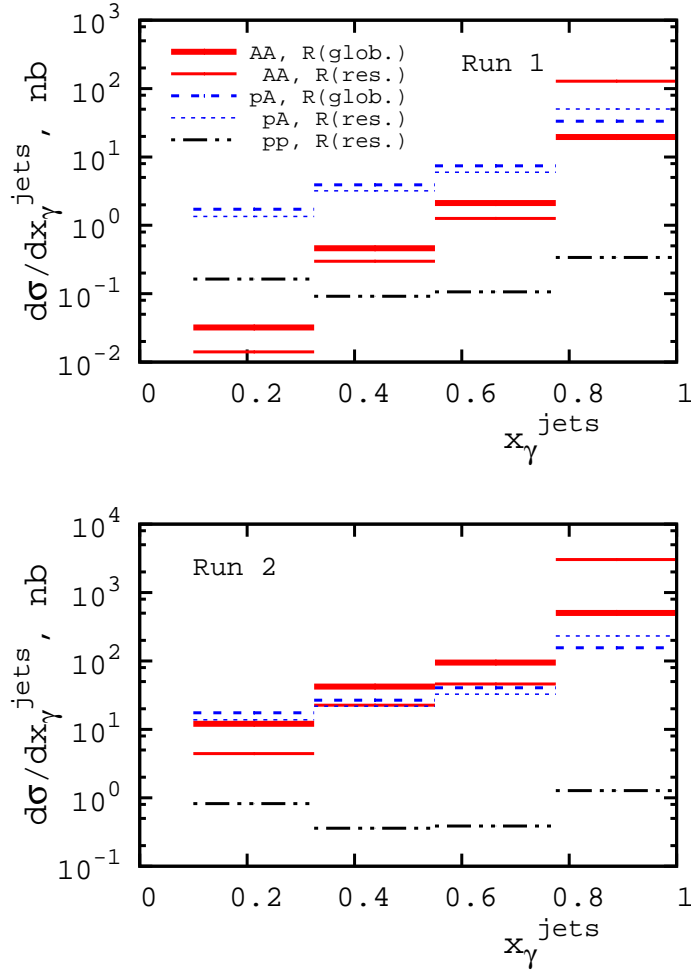


Figure 20. The x_{γ}^{jets} dependence of the cross section of diffractive dijet photoproduction in pp , pA and AA UPCs at the LHC during Run 1 (upper panel) and Run 2 (lower panel) calculated using the global (thick lines) and resolved-only (thin lines) schemes of factorization breaking.

The last equality gives a simple fit, which reproduces the calculation of f_p^{sup} to better than 5% accuracy. Note that $f_p^{\text{sup}}(x)$ gives the ratio of the red solid and the blue dot-dashed curves in the right panel of Fig. 6. The fit of Eq. (A.2) is valid both at $\sqrt{s_{NN}} = 5.02$ TeV and $\sqrt{s_{NN}} = 8.16$ TeV, since $f_p^{\text{sup}}(x)$ does not change in this energy interval to better than a fraction of a percent accuracy.

Acknowledgments

The authors would like to thank M. Strikman and M. Zhalov for carefully reading the manuscript and useful comments. VG would like to thank W. Vogelsang for useful discussions of photon PDFs and the Institut für Theoretische Physik, Westfälische Wilhelms-Universität Münster for hospitality. The work of VG is partially supported by a grant of

Deutscher Akademischer Austauschdienst (DAAD). The work of MK is partially supported by the BMBF Verbundprojekt 05H2015 through grant 05H15PMCCA.

References

- [1] E. Fermi, Z. Phys. **29** (1924) 315.
- [2] C. F. von Weizsäcker, Z. Phys. **88** (1934) 612; E. J. Williams, Phys. Rev. **45** (1934) 729.
- [3] V. M. Budnev, I. F. Ginzburg, G. V. Meledin and V. G. Serbo, Phys. Rept. **15** (1975) 181.
- [4] A. J. Baltz, G. Baur, D. d’Enterria, L. Frankfurt, F. Gelis, V. Guzey, K. Hencken and Y. Kharlov *et al.*, Phys. Rept. **458** (2008) 1.
- [5] M. G. Ryskin, Z. Phys. C **57** (1993) 89.
- [6] R. Aaij *et al.* [LHCb Collaboration], J. Phys. G **40** (2013) 045001.
- [7] R. Aaij *et al.* [LHCb Collaboration], J. Phys. G **41** (2014) 055002.
- [8] B. B. Abelev *et al.* [ALICE Collaboration], Phys. Rev. Lett. **113** (2014) 232504.
- [9] E. Abbas *et al.* [ALICE Collaboration], Eur. Phys. J. C **73** (2013) 2617.
- [10] B. Abelev *et al.* [ALICE Collaboration], Phys. Lett. B **718** (2013) 1273.
- [11] J. Adam *et al.* [ALICE Collaboration], Phys. Lett. B **751** (2015) 358.
- [12] S. P. Jones, A. D. Martin, M. G. Ryskin and T. Teubner, JHEP **1311** (2013) 085.
- [13] V. Guzey and M. Zhalov, JHEP **1310** (2013) 207.
- [14] A. Adeluyi and C. A. Bertulani, Phys. Rev. C **85** (2012) 044904.
- [15] V. Guzey, E. Kryshen, M. Strikman and M. Zhalov, Phys. Lett. B **726** (2013) 290.
- [16] T. Lappi and H. Mantysaari, Phys. Rev. C **87** (2013) 032201.
- [17] V. P. Goncalves, B. D. Moreira and F. S. Navarra, Phys. Rev. C **90** (2014) 015203.
- [18] S. Klein and J. Nystrand, Phys. Rev. C **60** (1999) 014903.
- [19] R. Aaij *et al.* [LHCb Collaboration], JHEP **1509** (2015) 084.
- [20] C. Adler *et al.* [STAR Collaboration], Phys. Rev. Lett. **89** (2002) 272302.
- [21] B. I. Abelev *et al.* [STAR Collaboration], Phys. Rev. C **77** (2008) 034910.
- [22] G. Agakishiev *et al.* [STAR Collaboration], Phys. Rev. C **85** (2012) 014910.
- [23] J. Adam *et al.* [ALICE Collaboration], JHEP **1509** (2015) 095.
- [24] L. Frankfurt, V. Guzey, M. Strikman and M. Zhalov, Phys. Lett. B **752** (2016) 51.
- [25] S. Chekanov *et al.* [ZEUS Collaboration], Eur. Phys. J. C **55** (2008) 177.
- [26] A. Aktas *et al.* [H1 Collaboration], Eur. Phys. J. C **51** (2007) 549.
- [27] F. D. Aaron *et al.* [H1 Collaboration], Eur. Phys. J. C **70** (2010) 15.
- [28] V. Andreev *et al.* [H1 Collaboration], JHEP **1505** (2015) 056.
- [29] M. Klasen and G. Kramer, Eur. Phys. J. C **38** (2004) 93.
- [30] M. Klasen and G. Kramer, Phys. Rev. Lett. **93** (2004) 232002.
- [31] M. Klasen and G. Kramer, J. Phys. G **31** (2005) 1391.

- [32] M. Klasen and G. Kramer, Mod. Phys. Lett. A **23** (2008) 1885.
- [33] M. Klasen and G. Kramer, Eur. Phys. J. C **70** (2010) 91.
- [34] T. Affolder *et al.* [CDF Collaboration], Phys. Rev. Lett. **84** (2000) 5043.
- [35] M. Klasen and G. Kramer, Phys. Rev. D **80** (2009) 074006.
- [36] G. Aad *et al.* [ATLAS Collaboration], Phys. Lett. B **754** (2016) 214.
- [37] M. Klasen, Rev. Mod. Phys. **74** (2002) 1221.
- [38] M. Klasen and G. Kramer, Proceedings of the 12th International Workshop on *Deep Inelastic Scattering* (DIS 2004), hep-ph/0401202.
- [39] W. Schäfer and A. Szczurek, Phys. Rev. D **76** (2007) 094014.
- [40] J. C. Collins, Phys. Rev. D **57** (1998) 3051 [Phys. Rev. D **61** (2000) 019902].
- [41] S. Chekanov *et al.* [ZEUS Collaboration], Eur. Phys. J. C **38** (2004) 43.
- [42] A. Aktas *et al.* [H1 Collaboration], Eur. Phys. J. C **48** (2006) 715.
- [43] A. Aktas *et al.* [H1 Collaboration], Eur. Phys. J. C **48** (2006) 749.
- [44] G. Ingelman and P. E. Schlein, Phys. Lett. B **152** (1985) 256.
- [45] C. A. Bertulani and G. Baur, Phys. Rept. **163** (1988) 299.
- [46] M. Vidovic, M. Greiner, C. Best and G. Soff, Phys. Rev. C **47** (1993) 2308.
- [47] M. Drees and D. Zeppenfeld, Phys. Rev. D **39** (1989) 2536.
- [48] B. A. Kniehl, Phys. Lett. B **254** (1991) 267.
- [49] J. Nystrand, Nucl. Phys. A **752** (2005) 470.
- [50] V. A. Khoze, A. D. Martin and M. G. Ryskin, Eur. Phys. J. C **18** (2000) 167.
- [51] K. A. Olive *et al.* [Particle Data Group Collaboration], Chin. Phys. C **38** (2014) 090001.
- [52] L. Frankfurt, C. E. Hyde, M. Strikman and C. Weiss, Phys. Rev. D **75** (2007) 054009.
- [53] M. Glück, E. Reya and A. Vogt, Phys. Rev. D **46** (1992) 1973.
- [54] M. Klasen, Nucl. Phys. Proc. Suppl. **207-208** (2010) 25 [arXiv:1007.1121 [hep-ph]].
- [55] L. Frankfurt, V. Guzey and M. Strikman, Phys. Rept. **512** (2012) 255.
- [56] V. Guzey and M. Zhalov, JHEP **1402** (2014) 046.
- [57] R. J. Glauber and G. Matthiae, Nucl. Phys. B **21** (1970) 135.
- [58] H. De Vries, C. W. De Jager and C. De Vries, Atom. Data Nucl. Data Tabl. **36** (1987) 495.
- [59] S. Chekanov *et al.* [ZEUS Collaboration], Eur. Phys. J. C **51** (2007) 301.
- [60] A. B. Kaidalov, V. A. Khoze, A. D. Martin and M. G. Ryskin, Eur. Phys. J. C **66** (2010) 373.
- [61] A. B. Kaidalov, V. A. Khoze, A. D. Martin and M. G. Ryskin, Phys. Lett. B **567** (2003) 61.
- [62] S. Aid *et al.* [H1 Collaboration], Nucl. Phys. B **463** (1996) 3.
- [63] J. Breitweg *et al.* [ZEUS Collaboration], Eur. Phys. J. C **2** (1998) 247.
- [64] T. H. Bauer, R. D. Spital, D. R. Yennie and F. M. Pipkin, Rev. Mod. Phys. **50** (1978) 261 [Rev. Mod. Phys. **51** (1979) 407].
- [65] V. Guzey and M. Strikman, Phys. Lett. B **633** (2006) 245 [Phys. Lett. B **663** (2008) 456].

- [66] V. Guzey, E. Kryshen and M. Zhalov, arXiv:1602.01456 [nucl-th].
- [67] V. Guzey and M. Strikman, Phys. Rev. C **75** (2007) 045208.
- [68] T. Altinoluk, N. Armesto, G. Beuf and A. H. Rezaeian, arXiv:1511.07452 [hep-ph].
- [69] R. Boussarie, A. V. Grabovsky, L. Szymanowski and S. Wallon, arXiv:1511.02785 [hep-ph].
- [70] R. Boussarie, A. Grabovsky, L. Szymanowski and S. Wallon, Acta Phys. Polon. Supp. **8** (2015) 897.